Results in Engineering 26 (2025) 105475

Contents lists available at ScienceDirect

Results in Engineering

journal homepage: www.sciencedirect.com/journal/results-in-engineering

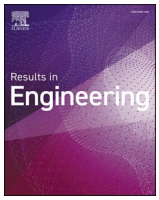

Research paper

# Predictive modeling of building energy consumption and thermal comfort for decarbonization in construction and retrofitting

Sameer Algburi [a], Aymen Mohammed [b,*], Ibrahim Abdullah [c], Talib Munshid Hanoon [d], Hassan Falah Fakhruldeen [e], Otabek Mukhitdinov [f], Feryal Ibrahim Jabbar [g], Qusay Hassan [h], Ali Khudhair [h], David Kato [h,*]

[a] College of Engineering, Al-Kitab University, Kirkuk 36015, Iraq
[b] Electrical Technical College, Al-Farahidi University, Baghdad, Iraq
[c] Computer Science Department, Al-Turath University College, Baghdad, Iraq
[d] Mazaya university college Iraq
[e] Computer Techniques Engineering Department, Faculty of Information Technology, Imam Ja'afar Al-Sadiq University, Baghdad 10011, Iraq
[f] Kimyo international university in Tashkent. Shota Rustaveli street 156 100121, Tashkent, Uzbekistan
[g] Medical Physics Department, College of Sciences, Al-Mustaqbal University 51001, Babil, Iraq
[h] College of Engineering, University of Deyala, Diyala, Iraq

ARTICLE INFO

*Keywords:*
Predictive energy modeling
Thermal comfort optimization
Net-zero carbon buildings
Building performance simulation
Monte Carlo
EnergyPlus analysis

ABSTRACT

This study introduces an integrated predictive modeling framework for assessing building energy consumption and indoor thermal comfort, with a focus on supporting decarbonization efforts in both new construction and retrofit scenarios. A total of 21 critical design and operational parameters were evaluated using Monte Carlo simulations combined with EnergyPlus, enabling high-resolution analysis of cooling loads, thermal comfort performance, and retrofit outcomes. The proposed multi-variable regression model demonstrated strong predictive accuracy, achieving an $R^2$ of 0.98, a mean absolute percentage error of 1.59 %, and a Coefficient of Variation of the Root Mean Square Error (CVRMSE) of 1.47 % in forecasting annual cooling demands. Optimization of variables such as indoor temperature set-point, solar heat gain coefficient, and glazing U-values yielded energy savings of up to 70 kWh/$m^2$ annually, corresponding to a potential carbon emission reduction of 31.5 kg $CO_2/m^2$/year, based on a regional electricity emission factor of 0.45 kg $CO_2$/kWh. The environmental quality thermal comfort index developed within this framework effectively quantified comfort conditions across varying scenarios, with values improving from 50 to 100 under optimized configurations. The model also revealed pronounced spatial variability, with perimeter zones reaching peak cooling loads of up to 198 W/$m^2$, emphasizing the need for zone-specific design strategies.

## 1. Introduction

A compelling impetus exists to adopt sustainable practices in construction and retrofitting, as highlighted by global climate initiatives such as the Net Zero Emission Pathway, which sets ambitious carbon reduction targets [1]. Achieving these targets necessitates advanced strategies in predictive energy modeling and enhanced design standards to minimize the environmental impact of both new and existing buildings [2,3]. Beyond compliance with tightening energy regulations, these strategies promote the integration of innovative technologies within the built environment. Elevating energy efficiency in building design serves as a vital mechanism for aligning industry practices with global energy reduction goals. Particular emphasis is placed on architectural design elements and socio-economic factors to support the holistic development of energy-efficient buildings [4]. This integrated approach expands the scope of energy efficiency benefits to encompass social equity and economic viability, enabling the implementation of technically grounded designs that address diverse community needs [5]. Such a framework contributes to sustainable development objectives and enhances urban resilience.

Within this global context, the pursuit of net-zero carbon buildings in Iraq reflects a national commitment to addressing climate change and modernizing the building sector. Central to this initiative is the

* Corresponding authors.
*E-mail addresses:* aymenaldulaimi@uoalfarahidi.edu.iq (A. Mohammed), kato@bose.uni.edu (D. Kato).

https://doi.org/10.1016/j.rineng.2025.105475
Received 19 February 2025; Received in revised form 30 March 2025; Accepted 23 May 2025
Available online 26 May 2025

**Abbreviations and Nomenclature**

| | |
|---|---|
| **ANN** | Artificial Neural Network |
| **ASHRAE** | American Society of Heating, Refrigerating and Air-Conditioning Engineers |
| **BIC** | Bayesian Information Criterion |
| **CDD** | Cooling Degree Days |
| **CFD** | Computational Fluid Dynamics |
| **CDH** | Cooling Degree Hours |
| **CVRMSE** | Coefficient of Variation of the Root Mean Square Error |
| **EQTC** | Environmental Quality Thermal Comfort |
| **GSR** | Global Solar Radiation |
| **HVAC** | Heating, Ventilation, and Air Conditioning |
| **IDF** | Input Data File |
| **kWh/m²** | Kilowatt-hours per square meter |
| **MAPE** | Mean Absolute Percentage Error |
| **MLR** | Multi-Linear Regression |
| **MRT** | Mean Radiant Temperature |
| **OFAT** | One-Factor-at-a-Time |
| **PMV** | Predicted Mean Vote |
| **PPDI** | Predicted Percentage of Dissatisfied Index |
| **$R^2$** | Coefficient of Determination |
| **SHGC** | Solar Heat Gain Coefficient |
| **SRC** | Standardized Regression Coefficient |
| **TMY** | Typical Meteorological Year |
| **UBEM** | Urban Building Energy Model |
| **U-value** | Thermal Transmittance ($W/m^2 \cdot K$) |
| **WE** | Weighted Exceedance Hours |
| **WAP** | Weighted Average Prediction |
| **Wh/m²** | Watt-hours per square meter |

enhancement of energy performance in the existing building stock, which typically exhibits inefficiency and elevated carbon emissions [6,7]. Retrofitting efforts involve deploying low-energy technologies and incorporating advanced materials and design practices. In new constructions, emphasis is placed on precise energy-use prediction through simulation tools such as EnergyPlus and e-QUEST, which enable performance optimization during the design phase [8]. Regulatory advancements further mandate high-efficiency standards across both existing and new buildings, driving adoption of modern technologies that reduce overall energy consumption [9].

### 1.1. Literature review

The imperative to decarbonize the building environment has drawn significant attention due to the pressing need to address climate change and enhance sustainability across both construction and retrofitting sectors. Within this framework, predictive modeling of building energy consumption and thermal comfort has become a central area of investigation. Increasingly, research efforts aim to integrate advanced technologies with empirical data to improve the precision of predictions, thereby informing strategies that facilitate the transition toward net-zero carbon buildings. Deb and Schlueter [10] conducted a comprehensive review of data-driven modeling techniques applied to building retrofit scenarios, demonstrating the efficiency of various statistical and machine learning methods in forecasting and optimizing energy performance post-intervention. Albatayneh et al. [11] examined the critical influence of thermal comfort models on energy consumption prediction, underscoring their importance in sustainable building design. The findings, published in Sustainability, highlight the extent to which divergent thermal comfort models can yield substantially different energy predictions, directly impacting decisions related to construction and retrofit planning. A key outcome of the study emphasizes the necessity for standardization in the application of thermal comfort frameworks to enhance the reliability of energy prediction models.

In the pursuit of practical decision-making tools, Saad et al. [12] explored surrogate modeling techniques with a focus on multi-criteria analysis to support retrofitting strategies within decarbonization efforts. These models simplify complex decision-making processes by providing quantitative estimates of cost-benefit relationships among retrofitting alternatives, offering substantial value to policymakers and developers seeking to balance environmental and economic priorities. Arowoiya et al. [13] investigated the integration of digital twin technology for improving both energy efficiency and thermal comfort in buildings. The study presented a state-of-the-art digital solution capable of producing dynamic, predictive performance models, illustrating the direction of future innovations in the field. Results indicate that digital twins represent a transformative advancement in predictive modeling by enabling real-time simulation and monitoring, which can significantly enhance both design and operational outcomes. Alghamdi et al. [14] developed a computational model that combines Monte Carlo simulation, EnergyPlus, and Artificial Neural Networks (ANN) to optimize predictions of energy consumption and thermal comfort. The model demonstrated strong performance, with $R^2$ values exceeding 0.97 for both energy consumption and thermal discomfort metrics during training and testing phases. Field validation further confirmed its reliability, with mean relative errors of $<2.0$ % for total energy use and below 1.0 % for average thermal discomfort hours. These findings collectively underscore the rapid evolution of predictive tools in building energy research and highlight the importance of integrating comfort and performance metrics into unified, high-accuracy models.

Energy performance and indoor thermal comfort in residential buildings, evaluated at both neighborhood and city scales, constitute foundational elements of urban design and planning. These factors exert substantial influence on environmental sustainability and the overall quality of life for urban populations. Energy performance encompasses the efficient application of energy resources to satisfy essential building functions such as heating, cooling, and lighting, while minimizing energy consumption and maintaining comfort standards. Indoor thermal comfort, by contrast, is determined by a building's internal environmental conditions, including air temperature, humidity, and airflow. These parameters must align with physiological and psychological thresholds to ensure occupant well-being. Braulio-Gonzalo et al. [15] introduced a methodology designed to predict energy performance and indoor thermal comfort across extensive residential building stocks at urban scales. A case study conducted in Spain demonstrated the integration of historical energy consumption data with simulation tools for assessing and enhancing energy efficiency. The resulting methodology offered urban planners a scalable framework aligned with long-term sustainability goals for residential districts. Santamouris et al. [16] examined current and future challenges related to building energy consumption, emphasizing the urgency of decarbonization. The study identified key drivers of energy demand and presented a comparative analysis of decarbonization strategies, weighing their benefits and trade-offs.

Gabrielli and Ruggeri [17] developed an innovative model aimed at simplifying the retrofitting process for large building portfolios. The proposed model incorporated energy assessment tools and optimization algorithms to formulate effective retrofitting strategies. An uncertainty analysis component was included to evaluate the robustness of the model against unpredictable variables affecting energy performance. Rabani et al. [18] designed an integrated optimization framework that combined building energy simulation with computational fluid dynamics and daylight analysis. This multi-faceted approach enabled optimization of building envelope design, fenestration configuration,

and HVAC system parameters, resulting in substantial energy savings and enhanced occupant comfort. Two retrofit scenarios were applied to a generic office building located in Oslo, Norway, yielding reductions in total energy consumption by 77 % and 79 %, respectively, along with significant improvements in both thermal and visual comfort metrics. Jafarpur and Berardi [19] investigated the effects of climate change on energy consumption and thermal comfort in office buildings situated within Canada's diverse climatic zones, including extremely cold, cold-humid, and cool-humid regions. The study revealed region-specific variations in projected temperature increases and their impact on building energy use. While heating demands were expected to decline, corresponding increases in cooling requirements were observed. Adjustments to thermostat setpoints demonstrated potential reductions in annual energy consumption, ranging from 0.9 % to 8.7 % in Quebec City, 1.6 % to 9.1 % in Toronto, and 1.4 % to 9.9 % in Vancouver. These findings underscore the importance of climate-responsive building design and retrofitting strategies in mitigating future energy burdens across varying geographic contexts.

Building envelope retrofitting involves modifications to the external components of a structure including walls, roofs, windows, and doors with the objective of enhancing energy efficiency and improving indoor comfort. Such interventions can yield substantial energy savings by reducing the operational demands placed on heating and cooling systems, thereby lowering overall energy consumption and associated costs. Martín-Consuegra et al. [20] present a comprehensive study focused on energy savings and thermal comfort improvements achieved through envelope retrofitting. The methodology integrates detailed data monitoring, occupant feedback through surveys, and simulation-based energy assessments to evaluate retrofit effectiveness. A key aspect of the study is the comparison between energy savings projected by standardized energy certificates and the actual post-retrofit consumption data. Findings reveal notable discrepancies: while heating savings were less than anticipated approximately a 25 % reduction cooling energy consumption was reduced by up to 50 %, exceeding expectations. Araújo et al. [21] address the challenge of stakeholder involvement in the retrofitting process, particularly in the context of Évora, Portugal, where procedures have often been perceived as rigid and bureaucratic. The study introduces a user-friendly, open-source interface designed to support informed decision-making throughout the retrofit lifecycle. The predictive model developed demonstrates high accuracy, with coefficients of determination reaching 0.84 and 0.79 for energy prediction metrics, highlighting significant potential for both energy reduction and financial return.

Mui et al. [22] contribute a hybrid simulation model tailored to estimate residential cooling energy demands specific to Hong Kong's climatic and architectural conditions. The model integrates multiple simulation methodologies to enhance precision, offering valuable insights for urban planners and engineers seeking to refine cooling strategies in dense, high-rise residential environments. Walker et al. [23] investigate the influence of contextual variables on retrofit decision-making across different European regions. The study emphasizes that the effectiveness of retrofitting strategies is highly dependent on regional climatic patterns, building typologies, and the regulatory landscape. Findings provide actionable guidance for customizing retrofit plans to regional circumstances, thereby increasing their potential for decarbonization impact. Aruta et al. [24] examine the application of advanced computational approaches—including genetic algorithms (GA) and ANN in model predictive control for heating systems in nearly zero-energy buildings. The methodology utilizes EnergyPlus weather datasets to simulate thermal behavior across economically varied winter conditions. Simulation results indicate that the optimized predictive control strategy achieved up to 26 % energy savings on the coldest, most energy-intensive day, February 28, compared to conventional fixed setpoint controls. These outcomes confirm the effectiveness of intelligent control algorithms in maintaining occupant comfort while advancing sustainable energy management practices in the building sector.

Minimizing energy consumption and decarbonizing building operations constitute essential strategies for reducing the environmental impact of the built environment and combating climate change. Effective implementation requires integration of energy-efficient technologies and advanced design measures such as enhanced insulation, high-performance heating and cooling systems, and intelligent control mechanisms that manage real-time energy use. Shi et al. [25] assessed the decarbonization potential of China's building sector using the China TIMES model, projecting an increase in energy use to 41.6 exajoules (EJ) by 2050 under a baseline scenario, with the potential to reduce this by up to 4 EJ through insulation improvements and technological advancements. Jradi et al. [26] introduced a digital twin framework to optimize retrofit decisions in Denmark's non-residential building stock, providing tools for energy performance enhancement, retro-commissioning, and policy guidance. Mata et al. [27] examined the economic feasibility of building retrofits in Sweden under five climate scenarios, concluding that near-term energy savings and upfront investment costs have a greater influence on profitability than long-term climatic uncertainties, particularly for strategies targeting space heating demand. González et al. [28] evaluated the impact of future climate conditions on historic buildings in Southern Europe, forecasting a 50 % rise in energy consumption to preserve human and artifact comfort, and underscoring the need for climate-adaptive retrofitting strategies. Dino and Akgül [29] investigated the implications of future overheating in Turkey, with simulations showing significant increases in cooling energy demand and reduced thermal comfort, reinforcing the urgency for system redesign and energy-sector decarbonization. Qu et al. [30] analyzed 63 passive retrofit strategies for a nineteenth-century Victorian residence in the United Kingdom, identifying vacuum-insulated glazing, infiltration control, and Polyisocyanurate insulation as the optimal combination, achieving a 51.8 % reduction in primary energy use and an 18-year payback period. Energy-saving and life-cycle decarbonization retrofitting of buildings encompasses comprehensive strategies aimed at minimizing energy use and reducing greenhouse gas emissions throughout the operational life of a structure. Cecconi et al. [31] developed a decision support system that utilizes low-cost, data-driven methods, including clustering techniques and Monte Carlo simulations, to identify optimal retrofit scenarios for over one million residential units, offering a scalable and adaptable solution under the EU Green Deal. S. Lin et al. [32] applied a calibrated urban building energy model (UBEM) with a 20 % prediction threshold to assess retrofitting of historic and modern buildings on a Chinese university campus, showing energy savings ranging from 10 % to 505 %, with the highest gains achieved through photovoltaic systems. Tamer et al. [33] conducted long-term forecasts of building performance in Turkey using data-driven models over a 60-year horizon, revealing significant increases in cooling demands and greenhouse gas emissions, particularly in warmer regions. Xu et al. [34] presented an optimization methodology for school buildings in Nanjing, China, combining building envelope analysis, energy systems, and occupancy data, achieving zero life-cycle carbon emissions through renewable integration and design efficiency. Thrampoulidis et al. [35] introduced a co-simulation and rolling-horizon forecasting model to test electricity demand flexibility during retrofitting, demonstrating that Swiss buildings can unlock considerable energy-use adaptability, essential for integrating intermittent renewable energy sources and improving energy management strategies.

Despite extensive research on energy efficiency and thermal comfort optimization, a significant gap remains in developing integrated models specifically designed for decarbonization in both new construction and retrofitting. Existing studies often address energy dynamics and comfort parameters in isolation, limiting their relevance for holistic building design and effective carbon mitigation strategies. Many current frameworks utilize advanced predictive analytics, yet lack the capacity for dynamic adaptation to real-time data and fluctuating environmental conditions. The absence of such adaptability restricts their utility in

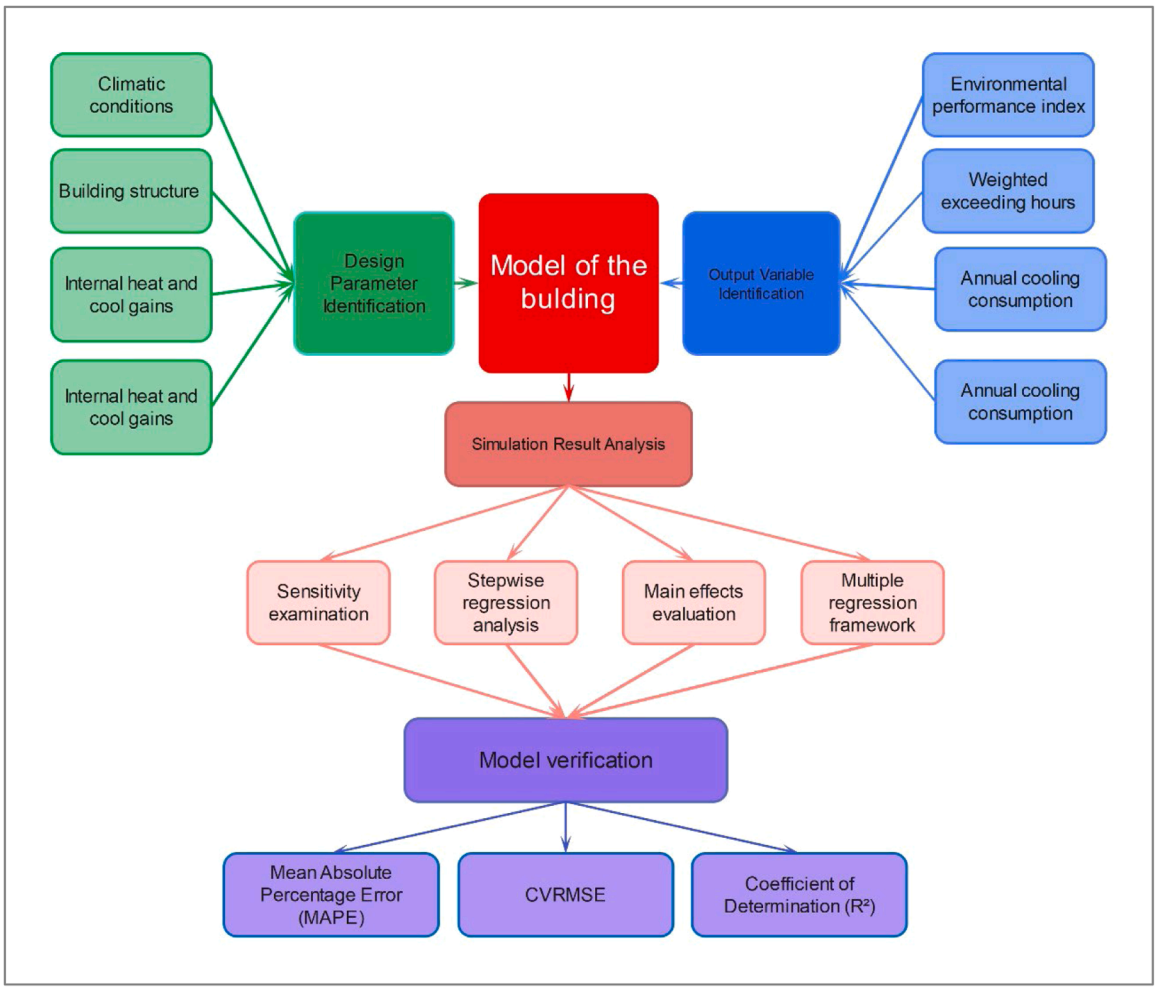


**Fig. 1.** Methodological framework for building energy performance simulation and analysis.

practical, performance-driven applications. This gap underscores the necessity for innovative predictive models that unify energy consumption and thermal comfort while accommodating changing usage patterns and climatic variability. A comprehensive, adaptable tool is essential to support decarbonization goals across diverse building typologies and operational contexts.

### *1.2. Study objective*

The objective centers on developing a data-driven predictive framework for accurately modeling building energy consumption and indoor thermal comfort to inform decarbonization strategies in both new construction and retrofitting. The framework integrates simulation tools and advanced statistical modeling techniques, including multivariable regression and machine learning, to evaluate energy performance under varying environmental and design conditions. Simulating different scenarios, the model enables quantitative assessment of energy demands and comfort outcomes, supporting optimized decisions regarding material selection, system configurations, and operational strategies. A core innovation lies in the unification of energy and comfort metrics into a single analytical system, offering dynamic, real-time adaptability to changing usage patterns and climatic inputs. The framework also provides a comparative analysis of retrofitting alternatives, allowing stakeholders to identify the most cost-effective and environmentally beneficial solutions. This integrative approach addresses gaps in existing literature by moving beyond isolated energy or comfort models and delivering a scalable tool aligned with sustainable design and net-zero carbon objectives.

The novelty of the study lies in the integration of building energy consumption and thermal comfort into a unified predictive modeling framework, addressing a longstanding gap in sustainable building research. Conventional approaches that treat these domains separately, the model employs advanced statistical and machine learning techniques to enable simultaneous assessment and optimization of both performance metrics. Real-time adaptability is embedded into the system, allowing dynamic responses to shifting climatic conditions and occupancy behaviors. The framework further distinguishes itself by simulating a broad spectrum of retrofitting strategies, offering predictive insights into cost-effectiveness and environmental impact. Incorporation of nonlinear dynamics and variable interactions enhances model accuracy and relevance, delivering a robust tool suitable for diverse climatic zones and building typologies. This integrated, data-driven approach establishes a scalable foundation for next-generation smart building design and decarbonization planning.

## 2. Methodology

### *2.1. Building energy performance*

A structured simulation and analytical approach were followed in the building energy performance as illustrated by the flowchart presented in Fig. 1. First, design parameters such as internal gains, building physics, climatic conditions, and ventilation are identified and integrated into a building model. The model is important in determining

critical output variables. These variables are important in determining indoor thermal comfort and the overall energy efficiency of the building.

The methodology bifurcates into two distinct paths: firstly, Monte Carlo simulations are carried out with random sampling in order to create multiple EnergyPlus Input Data Files (IDF), allowing for the deep examination of possible building performance scenarios under diverse conditions [36,37]. These results from simulations then undergo rigorous processing in sensitivity analysis, main effects analysis, and stepwise regression to determine the important predictors and interactions affecting building performance. One further applies a multiple regression model so as to set up simplified linear prediction equations describing the nonlinear relations between design parameters and energy performance outputs [38,39].

The mathematical model in the study, however, is a multiple regression model that goes further than mere linear estimation of understanding complex relationships between input variables and predicted outcomes. This model is designed to explain not only the direct effects of individual variables but also to capture nonlinear impacts and interactions between different variables. These enhancements permit more detailed, accurate modeling of the interactive influences of some factors such as material properties and environmental conditions on building energy performance. Such a model is crucial for developing better performing building designs through an improved understanding of the interactions among all the elements impacting cooling load and, ultimately, in improving energy standards and building practices described as:

$$U = \alpha + \sum_{i=1}^{k} a_i z_i + \sum_{i=1}^{k} b_i z_i^2 + \sum_{i=1}^{k-1} \sum_{j=i+1}^{k} c_{ij} z_i z_j + \epsilon \tag{1}$$

where, $U$ is the predicted output, $z_i$ is the $i^{th}$ input, $\alpha$ is the intercept of the relationship, $\alpha_i$, $b_i$, and $c_{ij}$ are the regression coefficients for the linear, quadratic, and interaction terms respectively, and $\epsilon$ is the term of error.

A black-box model, therefore, helps in the analysis of building design strategies using historical data to make forecasts and understand the complicated relationships [40]. In this statistical approach, the outcome variable is modeled as a function of multiple independent variables capturing both direct and interactive effects. It is referred to as a black-box model because it pays attention only to the input-output relations and does not give clear, mechanistic insight into how the internal system works. Analyzing past performance data of buildings helps in deriving predictive insights through such models, which can be put to use for optimizing future building designs toward improved energy efficiency and performance.

Monte Carlo analysis takes this further and complements the same by using statistical sampling techniques to effect robust simulations using a range of inputs, all drawn from probability distributions in modeling different scenarios related to building designs [41]. This is fundamental to understanding how uncertainties in the input variables arising from several sources such as material properties, climate, and usage patterns may affect the building's performance. Each time a simulation is run, possible outcomes are created based on random sampling, and these collectively form a probability distribution of possible outcomes. Which offer designers and engineers a probabilistic view of building performance and allow the formulation of design strategies that are resilient and optimized under a range of possible conditions. The inclusion of quadratic terms in the model allows for consideration of nonlinear dynamics between variables, while the interaction terms reveal how the interplay between pairs of variables affects the outcome. These interaction terms help to explicate how the Solar Heat Gain Coefficient (SHGC) of glass combined with the window area affects the cooling load, describe as:

$$U = \begin{bmatrix} w_1 \\ w_2 \\ . \\ . \\ . \\ w_M \end{bmatrix} \begin{bmatrix} G_1(u_{11}, u_{12}, \ldots, u_{1j}) \\ G_2(u_{21}, u_{22}, \ldots, u_{2j}) \\ . \ . \ . \ . \ . \ . \\ . \ . \ . \ . \ . \ . \\ . \ . \ . \ . \ . \ . \\ G_M(u_{M1}, u_{M2}, \ldots, u_{Mj}) \end{bmatrix} \tag{2}$$

where, $G_i$ be the function representing the relationship between inputs and the output for each observation *i*, $M$ be the matrix size, $j$ the input factors number, $u_{ij}$ be the input variables, and $w_i$ be the output variable for each observation.

This work intends to assess the impact on four different outputs: Peak Cooling Load, the maximum instantaneous cooling demand for an overall considered period of time; Annual Cooling Load, that considers the total cooling energy need; Weighted Exceeding Hours, the number of hours during which an indoor environment violates specific comfort limits; and an overall indicator named EQTC, standing for Environmental Quality Indoor Thermal Comfort, to estimate the general indoor environment quality about the considered thermal environment. Moreover, such outputs are very important for green building certification because directly related to that are the criteria of energy efficiency and environmental impact, which constitute parts of any certification standard [42,43]. The choosing and defining of input parameters of building simulation models is a pivot point since the accuracy and relevance of analysis strongly depend on them.

This complexity becomes apparent due to the many variables affecting building performance, as all are interacting with each other in a dynamic built environment. The parameters include building geometry, which determines the spatial characteristics and surface area exposed to environmental conditions that affect energy demands for heating and cooling [44]. The envelope thermo-physics is a factor involving thermal properties of materials used in building walls, roofs, and windows, which determine heat transfer rates and thus influence thermal loads and comfort levels inside the building [45]. The other major input parameter is HVAC system operation, including efficiency, design, and control systems of heating, ventilation, and air conditioning units [46]. They are imperative for indoor environmental quality and comfort, and the way they can function can hugely vary depending on a building's design and patterns of use. Weather conditions become a basic parameter since variations in temperature, humidity, solar radiation, and wind can all hugely change a building's thermal loads [46]. Architectural and engineering practices therefore impact the choice of technologies, design standards, and operational strategies that all determine how the building performs under various scenarios [47,48]. Those practices now integrate the concepts of sustainability and the innovations in building technology to reduce energy consumption while improving the comfort and health of building occupants. Those are the factors that require much attention and should be modeled accurately to ensure the simulations are realistic and add value to building design and operation.

### 2.2. Evaluation of indoor thermal comfort using EQTC

The EQTC metric offers a detailed assessment of both environmental and physiological parameters to evaluate indoor thermal comfort, ensuring alignment with occupant needs. Utilizing the Predicted Mean Vote (PMV) and Predicted Percentage of Dissatisfied (PPD) indices widely recognized thermal comfort measures EQTC bases its predictions on six key variables: clothing insulation, air velocity, metabolic activity, air temperature, relative humidity, and mean radiant temperature (MRT) [49,50]. Standardized inputs within the model assume a clothing insulation value of 0.55 clo, reflecting typical indoor conditions, and an air velocity of 0.15 m/s to represent gentle airflow [51,52]. Simulation

**Table 1**
Categorization and weighting of thermal comfort levels in EQTC assessment.

| Category | PMV Range | Weight | Description |
|---|---|---|---|
| I | [−0.1, +0.1] | 100 | Most comfortable, highest weight |
| II | [−0.3, +0.3] | 75 | Moderately comfortable |
| III | [−0.5, +0.5] | 40 | Least comfortable, lower weight |

**Table 2**
EQTC rating levels and score intervals.

| Rating level | Interval of EQTC |
|---|---|
| Level A | 100–90 |
| Level B | 90–75 |
| Level C | 75–60 |
| Level D | 60–45 |
| Level E | 45–30 |
| Level F | 30–15 |
| Level G | 15–0 |

and analysis of these parameters are conducted using advanced building performance software such as EnergyPlus, allowing for high-resolution environmental modeling [53]. To assess performance across seasonal variations, the model calculates the percentage of time indoor conditions remain within defined thermal comfort classes, as outlined in Table 1. This approach enables year-round evaluation of continuous PMV values under a range of climatic and operational scenarios [54,55].

Thermal comfort conditions within a building can be systematically classified and quantified based on the frequency with which indoor environments remain within occupant-accepted comfort ranges. This classification framework incorporates multiple comfort levels, each assigned a specific weight to reflect its relative desirability or acceptability. The cumulative sum of these weighted comfort levels forms the basis of the EQTC assessment, providing a comprehensive measure of a building's effectiveness in sustaining optimal thermal comfort over a defined period.

Eq. (3) in the model provides a formula for calculating the EQTC, which integrates varying levels of comfort into a single metric.

$$EQTC = I \times 100 + II \times 75 + III \times 35 \tag{3}$$

Table 2 show the EQTC uses system levels to evaluate the thermal environment within a space, ranging from 0 to 100. This index divides into seven rating levels, each representing a different range of comfort.

During the evaluation process, the exceedance metric identifies each instance within a specified period such as a day or a year when indoor temperature surpasses the defined comfort threshold for a duration of at least one hour. In addition to frequency, the metric also accounts for the severity of exceedance, quantifying temperature deviations above the comfort range by specific margins, such as 1 °C or 5 °C..

$$WE = \frac{\sum_{i=1}^{n} v_i h_i}{355} \text{where} v_i = \begin{cases} \dfrac{PPDI_i}{PPDI_{\max}} & if\ PMV_i \geq 0.5 \\ 0 & otherwise \end{cases} \tag{4}$$

where, $WE$ represent the duration of weighted exceedance, $v_i$ as the weighting factor for each time step, $h_i$ to represent the time step in hours, $PPDI_i$ as the PPDI at each time step, and $PPDI_{\max}$ as the limit for comfort of PPDI.

### 2.3. Simulation model of a multi-floor open office building layout

A detailed simulation model of a multi-story mid-rise office building was developed to evaluate energy efficiency and the influence of architectural design on sunlight modulation. The structure is segmented into clearly defined thermal zones, including core zones and perimeter areas on each floor, with the perimeter spaces being directly affected by external conditions through the façade. As shown in Fig. 2, the model integrates overhangs positioned above the windows, quantified by the overhang projection ratio (depth-to-height), which play a pivotal role in reducing direct solar gain. These passive shading elements are particularly effective in limiting heat gain during summer months while

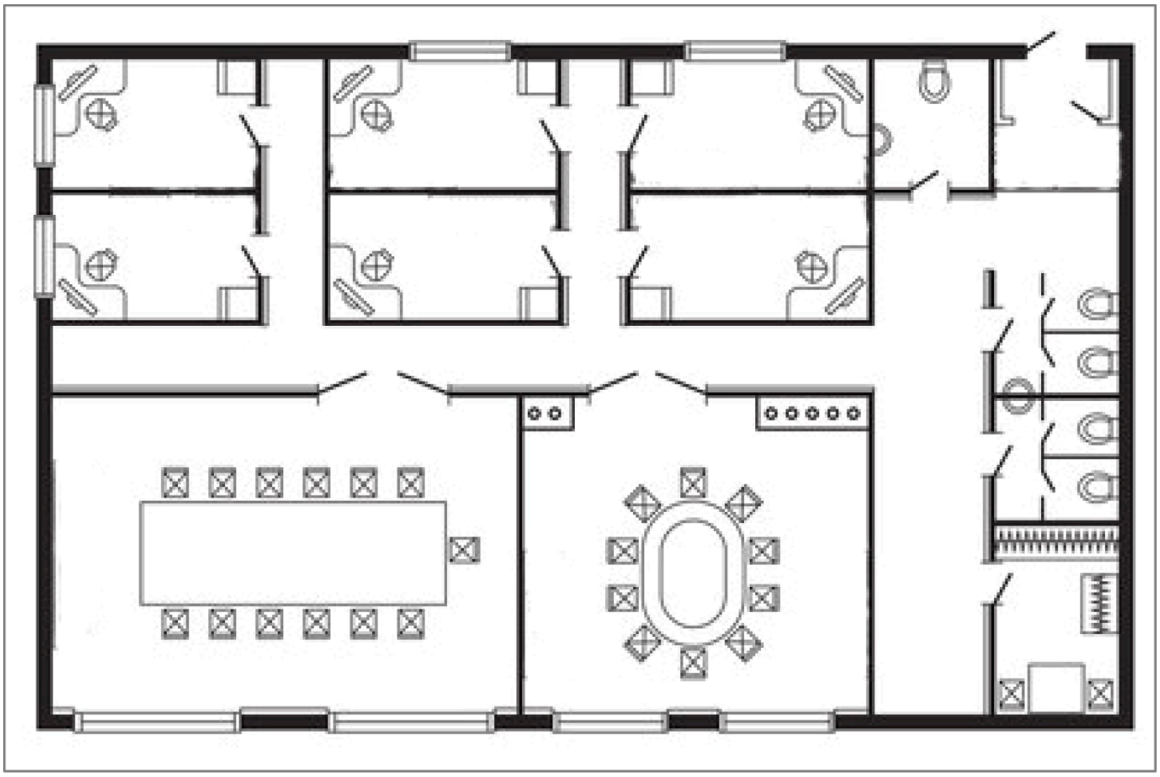

**Fig. 2.** Schematic representation of multi-floor open office building with overhang projection.

**Table 3**
Variables and their ranges in building design simulation.

| Design Features | Variable | Description | Range | Remarks |
|---|---|---|---|---|
| Climatic Conditions | $y_1$ | Max temp on design day | 33.5–35.5 °C | |
| | $y_2$ | Daily avg cooling degree hours | 55.6–65.6 °C-hour | |
| | $y_3$ | Daily avg global solar radiation | 4.3–5.8 Wh/m$^2$ | Applies to perimeter zones only |
| Building Envelope | $y_4$ | Aspect ratio | 0.6–2.5 | |
| | $y_5$ | Floor-to-ceiling height | 2.6–3.6 m | Applies to perimeter zones only |
| | $y_6$ | Building orientation | −180–180 degrees | For model validation N, E, S, W |
| | $y_7$ | Ratio of window to floor area | 0.25–0.55 | Applies to perimeter zones only |
| | $y_8$ | SHGC of glass | 0.31–0.77 | Applies to perimeter zones only |
| | $y_9$ | Thermal transmittance of glass (U-value) | 1.8–5.8 W/m$^2$·K | Applies to perimeter zones only |
| | $y_{10}$ | Projection ratio of overhang | 0.01 –1.2 | Applies to perimeter zones only |
| | $y_{11}$ | U-value of wall | 0.455–2.325 W/m$^2$·K | Applies to perimeter zones only |
| | $y_{12}$ | Thermal mass of wall | 300–700 kJ/m$^2$·K | Applies to perimeter zones only |
| | $y_{13}$ | Absorptance of wall exterior surface | 0.35–0.75 | Applies to perimeter zones only |
| Internal Heat Sources | $y_{14}$ | Thermal mass inside building | 35–190 kJ/m$^2$·K | |
| | $y_{15}$ | Power density of equipment | 8–25 W/m$^2$ | |
| | $y_{16}$ | Lighting power density | 5–18 W/m$^2$ | |
| | $y_{17}$ | Density of occupants | 0.06–0.18 person/m$^2$ | |
| | $y_{18}$ | Metabolic rate of occupants | 115–145 W/person | |
| Airflow Characteristics | $y_{19}$ | Air infiltration rate | 0.01–0.2 Air Changes / Hour | |
| | $y_{20}$ | Air ventilation rate | 0.45–1.55 l/s·m$^2$ | |
| Thermal Control | $y_{21}$ | Set-point of indoor temperature | 25.0–27.0 °C | |

**Table 4**
Climatic parameters for design day and typical meteorological year across selected three cities.

| Climate Data | Metric symbol | Baghdad | Mosul | Basra |
|---|---|---|---|---|
| Design Day Temperature | | | | |
| Dry- (Wet-) bulb at 0.4 % occurrence | *T* 0.5 % | 36.6 | 38.5 | 39.7 |
| Dry- (Wet-) bulb at 1.0 % occurrence | *T* 1.5 % | 35.4 | 34.2 | 34.4 |
| Dry- (Wet-) bulb at 2.0 % occurrence | *T* 2.5 % | 35.4 | 34.6 | 35.7 |
| Typical Meteorological Year Data | | | | |
| Hours of avg. daily cooling degree | *CDH* | 60.1 | 65.4 | 70.6 |
| Avg. daily solar radiation | *SR* | 4 | 4.5 | 4.5 |

permitting beneficial solar exposure during winter, when the sun's angle is lower. This passive design strategy significantly enhances indoor thermal comfort within perimeter zones. The configuration exemplifies how architectural interventions can be used to optimize natural daylighting, lower building energy demands, and improve occupant comfort across multiple floor levels.

The building model defined by a given side dimension of 40 m and an aspect ratio between 0.6 and 2.5 modifies the building depth with regard to its width in such a way that it can accommodate diverse site constraints and aesthetic preferences. It employs the 21 input variables listed in Table 3, covering a wide spectrum of design features crucial to the simulation and analysis of building thermal and energy dynamics.

Table 4 presents a comparative analysis of climatic parameters between design day conditions and typical meteorological year data for three major cities. Temperature values are reported across various percentiles, capturing the range from average to extreme heat conditions, and are accompanied by indicators related to cooling demand and solar radiation exposure.

### 2.4. Model validation

The model was validated using the following four key metrics: Coefficient of Variation of the Root Mean Squared Error (CVRMSE), Mean Absolute Percentage Error (MAPE), Weighted Average Prediction (WAP), and Coefficient of Determination ($R^2$) [56–58]. CVRMSE was used as a measure of the accuracy of the model predictions, relative to the scale of the observed data, thus showing the consistency of the model. MAPE measured the average size of the errors as a percentage, making it easy to interpret predictive accuracy. The WAP considered the importance of different predictions by weighting them, which gave a balanced assessment with varied data points. $R^2$ measured the proportion of variance in observed data explained by the model, giving an indication of the goodness-of-fit of the whole model.

$$CVRMSE(\%) = \frac{100}{D} \times \sqrt{\frac{\sum_{k=1}^{N}(d_k - p_k)^2}{N}} \tag{5}$$

$$MAPE(\%) = 100 \times \frac{1}{N}\sum_{k=1}^{N}\left|\frac{d_k - p_k}{d_k}\right| \tag{6}$$

$$WAP = \sum_{k=1}^{N}\left(\frac{S_k}{\sum_{j=1}^{N} S_j}\right) p_k \tag{7}$$

$$R^2 = \frac{\sum_{k=1}^{N}(p_k - D)^2}{\sum_{k=1}^{N}(d_k - D)^2} \tag{8}$$

where, $D$ is the mean of the actual values, $N$ is the total number of observations, $d_k$ is the actual data value for the $k^{th}$ observation, $p_k$ is the predicted data value for the $k^{th}$ observation, $S_k$ is the area of the $k^{th}$ space or unit, and $D$ is the mean of the actual data values

## 3. Results and discussions

The key findings derived from the simulation models, statistical analyses, and validation processes outlined in the methodology presented in this section. The performance of the proposed predictive framework is evaluated in terms of energy consumption, indoor thermal comfort, and sensitivity to architectural and climatic variables. Validation metrics are compared against relevant literature to assess accuracy and robustness, while parametric analyses explore the influence of design and operational factors. The results also highlight the effectiveness of passive design features, retrofitting scenarios, and zone-specific energy behavior, offering insight into optimized strategies for enhancing building energy performance and occupant comfort.

### 3.1. Nonlinear dynamics in MLR models through OFAT analysis

This section presents simulation results that offer critical insights into the nonlinear relationships between input variables and model

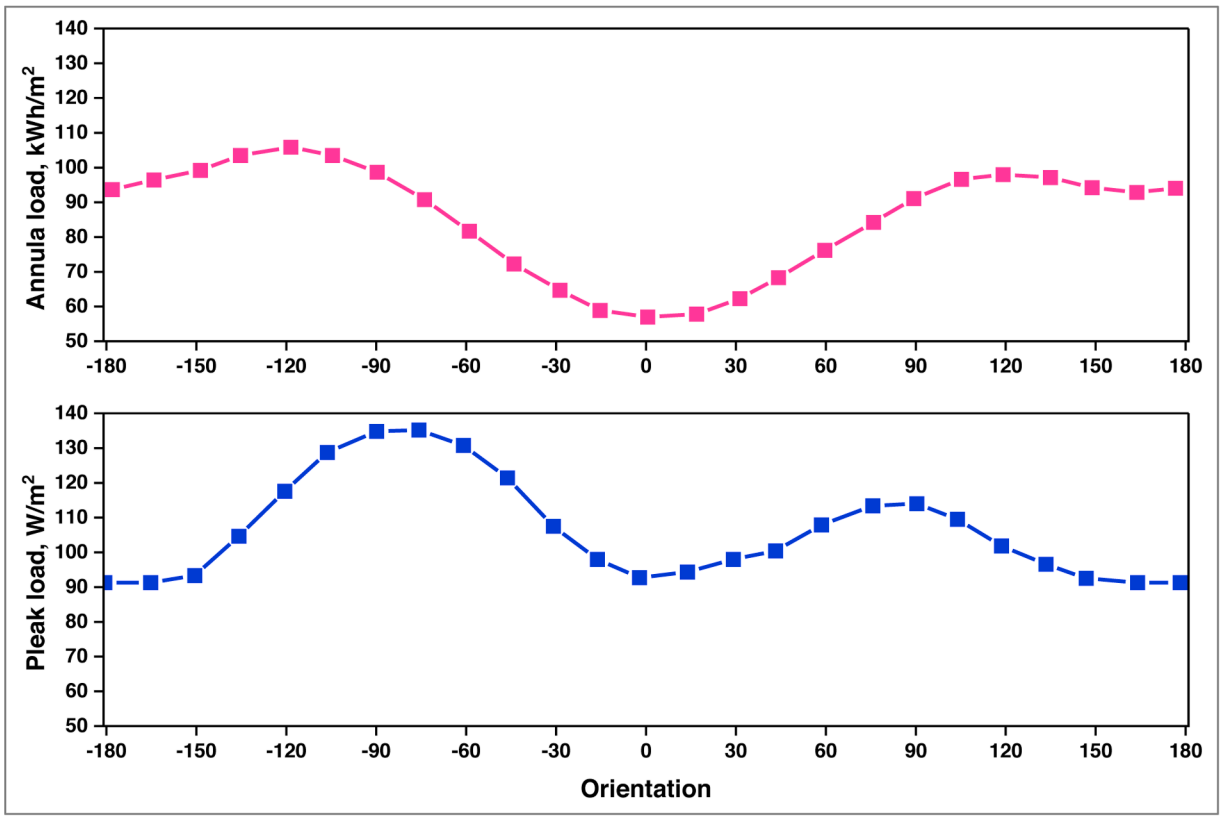


**Fig. 3.** Effect of building orientation on peak load.

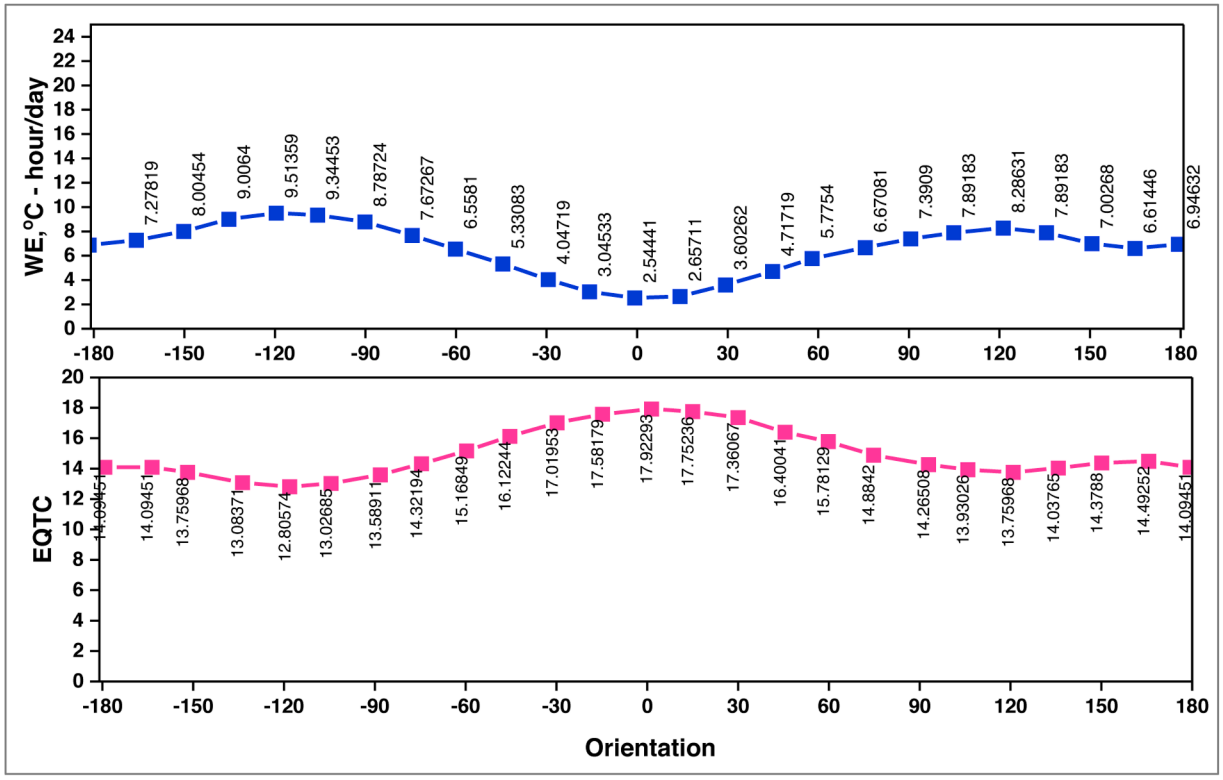


**Fig. 4.** Effect of building orientation on WE and EQTC.

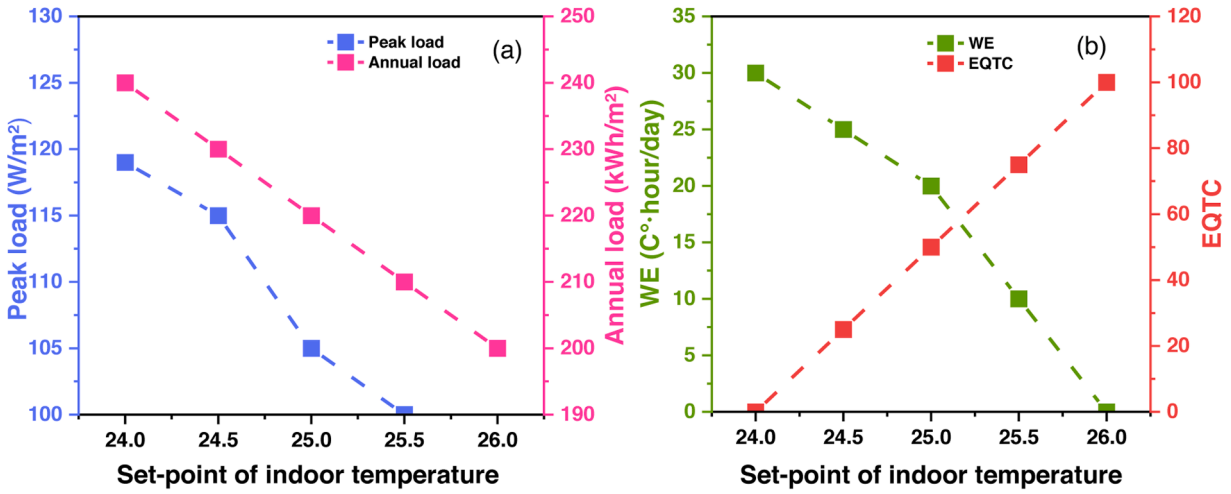


**Fig. 5.** Indoor temperature set-point (a) load, (b) WE and EQTC.

outputs. The OFAT method was employed by systematically varying individual input parameters while holding others constant, enabling an isolated assessment of each variable's influence on energy performance metrics [59,60]. This approach revealed complex interactions and nonlinear effects that are typically overlooked in conventional linear regression models. The analysis identified specific variables exerting strong nonlinear impacts on model predictions, reinforcing the necessity of incorporating nonlinear dynamics to ensure accurate representation of system behavior [61,62]. As illustrated in Fig. 3, the variation in both annual and peak cooling loads with respect to building orientation demonstrates a clear symmetrical trend. The annual load decreases from –180° to 0°, reaching a minimum at 0°, before rising again toward 180°, suggesting that deviations from this central orientation result in increased energy demands. Similarly, the peak load exhibits elevated values around –150° and –120°, followed by a decline toward 0°, and a subsequent rise approaching 180°. These findings highlight orientation as a key driver of energy performance, confirming the relevance of OFAT analysis for enhancing model precision and understanding the influence of baseline design parameters.

Fig. 4 presents the relationship between building orientation and two key performance indicators: EQTC and WEiTC. The top graph demonstrates that EQTC values generally range from approximately 12 to 18 h per day, with the highest performance occurring near 0° orientation. A gradual decline is observed as the orientation shifts toward –180° and 180°, where values reach their minimum. The lower graph illustrates a similar trend for WEiTC, which spans approximately 6 to 8 h per day. Peak values are again observed at 0°, while orientations at the extremes show reduced performance. These symmetrical patterns indicate that both thermal comfort metrics are optimized around the central orientation, with significantly diminished efficiency and control at peripheral angles, highlighting the importance of orientation in passive design strategies.

Fig. 5(a) shows the relation between indoor temperature set-point and peak and annual load. As the indoor temperature set-point rises from 24 to 26 °C, the peak load drastically drops from 125 W/m² to 95 W/m². A higher indoor temperature set-point tends to decrease the cooling demand during the peak time. The annual load also decreases with an increase in indoor temperature set-point: from 240 kWh/m² at 24 °C to 200 kWh/m² at 26 °C. A clear trend arising here is that the higher the indoor temperature set-point maintained for the whole year, the larger the energy saved. Fig. 5(b) shows the dependence of WE and EQTC on indoor temperature set-point. As the indoor temperature set-point increases, WE decrease from 30 C°·hour/day at 24 °C to 0 C°·hour/day at 26 °C, which is indicative of a direct relationship between higher temperature set-points and reduced thermal discomfort. On the contrary, EQTC rises with increased indoor temperature set-points, rising from 0 at 24 °C to 100 at 26 °C.

Fig. 6(a) indicates the variation in peak and annual load due to SHGC. Peak and annual loads increase linearly with increasing SHGC from 0.4 to 0.9. In fact, the peak load increases from 100 W/m² at an

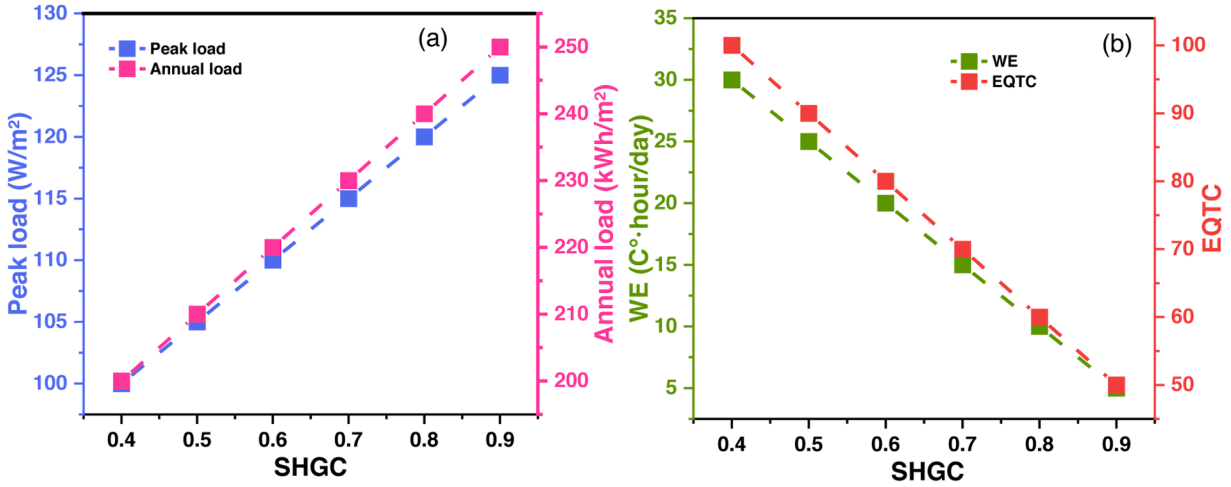


**Fig. 6.** The SGH (a) annual load and peak load, (b) EQTC and WE.

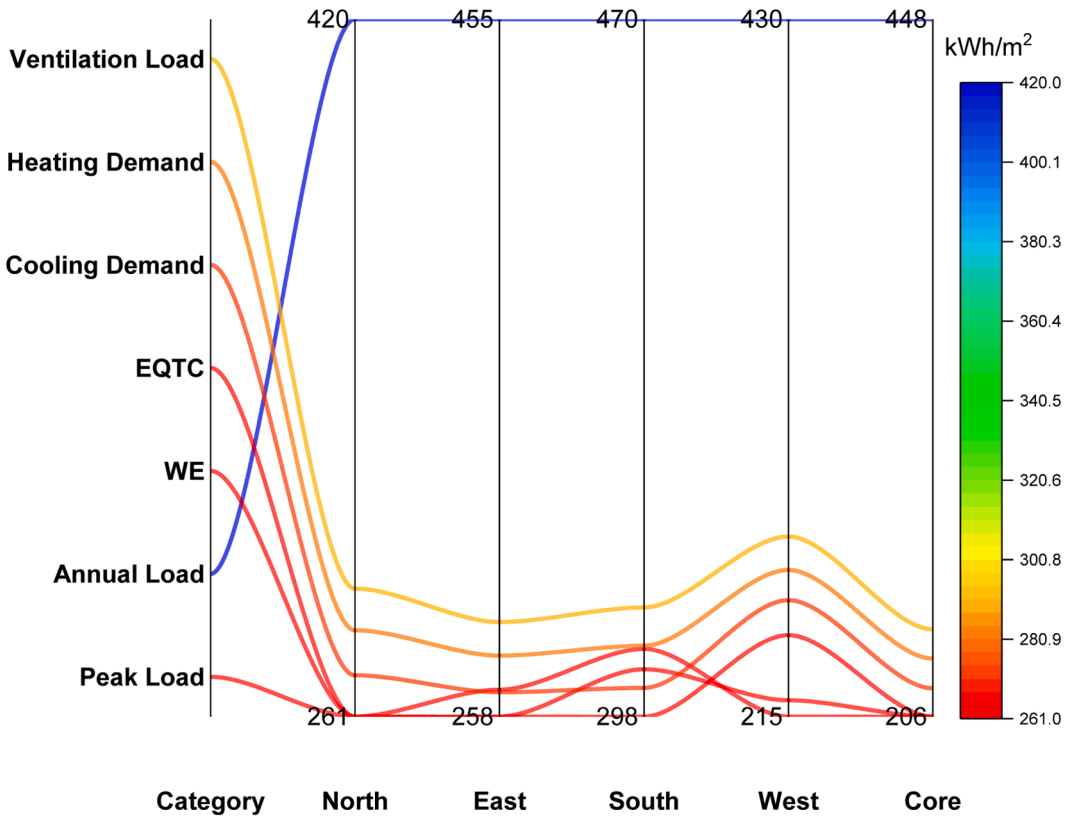


**Fig. 7.** Simulation indicators of annual energy loads and thermal comfort.

SHGC of 0.4 to 125 W/m$^2$ at an SHGC of 0.9. The annual load also rises from 200 kWh/m$^2$ to 250 kWh/m$^2$ within the same range of SHGC. These trends mean that higher SHGC values, relating to more solar heat gain via windows, result in significant increases in cooling demand and overall energy consumption. Fig. 6(b) presents the tendency of SHGC with WE and EQTC: as SHGC increases from 0.4 to 0.9, WE decrease from 30 C°·h/day to 5 C°·h/day, showing a decline in the state of thermal discomfort as the SHGC increases. On the other hand, EQTC drops from 100 to 50 with an increase in SHGC, indicating a drop in the thermal comfort index.

### 3.2. Spatial energy and thermal load simulations results

These outputs emulate a detailed energy performance of all building zones using EnergyPlus and Monte Carlo experiments. The result shows large differences in design peak loads and annual energy loads in perimeter compared to core zones. Specifically, the design peak load for the perimeter areas is between 54 and 198 W/m$^2$, while core areas have a peak load of between 42 and 106 W/m$^2$, as shown in Fig. 7. This difference shows that the cooling loads of the perimeter zones are normally higher than those of core areas since they are directly exposed to outside thermal conditions.

Significant disparities are observed in annual energy loads between core and perimeter zones, with perimeter zones exhibiting a range from 152 to 506 kWh/m$^2$, while core zones range between 142 and 395 kWh/m$^2$. These variations have critical implications for energy management, emphasizing the necessity for zone-specific HVAC strategies to achieve optimized energy performance. In addition, the WE daily average metric serves as a valuable indicator for evaluating thermal comfort levels across different zones and for tracking temporal shifts in indoor environmental conditions throughout the day.

The EQTC values provide fundamental information concerning thermal comfort inside the building. Greater variability in EQTC values for perimeter areas compared to core areas indicates a greater need for dynamic and responsive climate control systems in the perimeter zones. This is very important for keeping indoor thermal comfort constant, hence improving the satisfaction of the occupants and reducing energy consumption. The obtained simulation results underline the importance of the distinction between core and perimeter areas for effective energy and comfort control.

Comparing the results, clear differences between core and perimeter areas in building thermal comfort indicators can be appreciated. Core areas: WE range between 0 and 36 h/d, indicating that this area would generally have a more stable thermal environment compared with the perimeter areas, which showed a WE ranging from 0 to 45 h/d. Such variability of the perimeter areas is due to their exposure in outside temperature oscillations, aside from sunlight absorption, hence it causes surface temperatures to rise—thereby making thermal comfort management at the perimeter areas difficult to manage and becoming more dynamically controlled through HVAC systems. This also manifests through the EQTC scores, as all values pertain to an overall range between 0 and 100 in both the core and perimeter zones. Nevertheless, with a surge in the temperatures along the perimeter zones, high values for PMV and PPDI demonstrate increased risks of suffering thermal discomfort. It is clear that such disparities require targeted strategies because maintaining consistent indoor comfort in the perimeter zones is vital for overall building efficiency and the comfort of occupants.

### 3.3. Sensitivity analysis results

Sensitivity analysis results, as illustrated in Fig. 8, reveal that different input parameters exert varying levels of influence on annual cooling load, peak load, work efficiency, and EQTC across perimeter and core zones. These variations highlight the zone-specific impact of design and operational factors on thermal and energy performance outcomes.

The peak load results show that the perimeter and core zones are sensitive to different extents by various parameters (y1 to y21). For the perimeter zones, the sensitivity coefficient values vary between −0.1

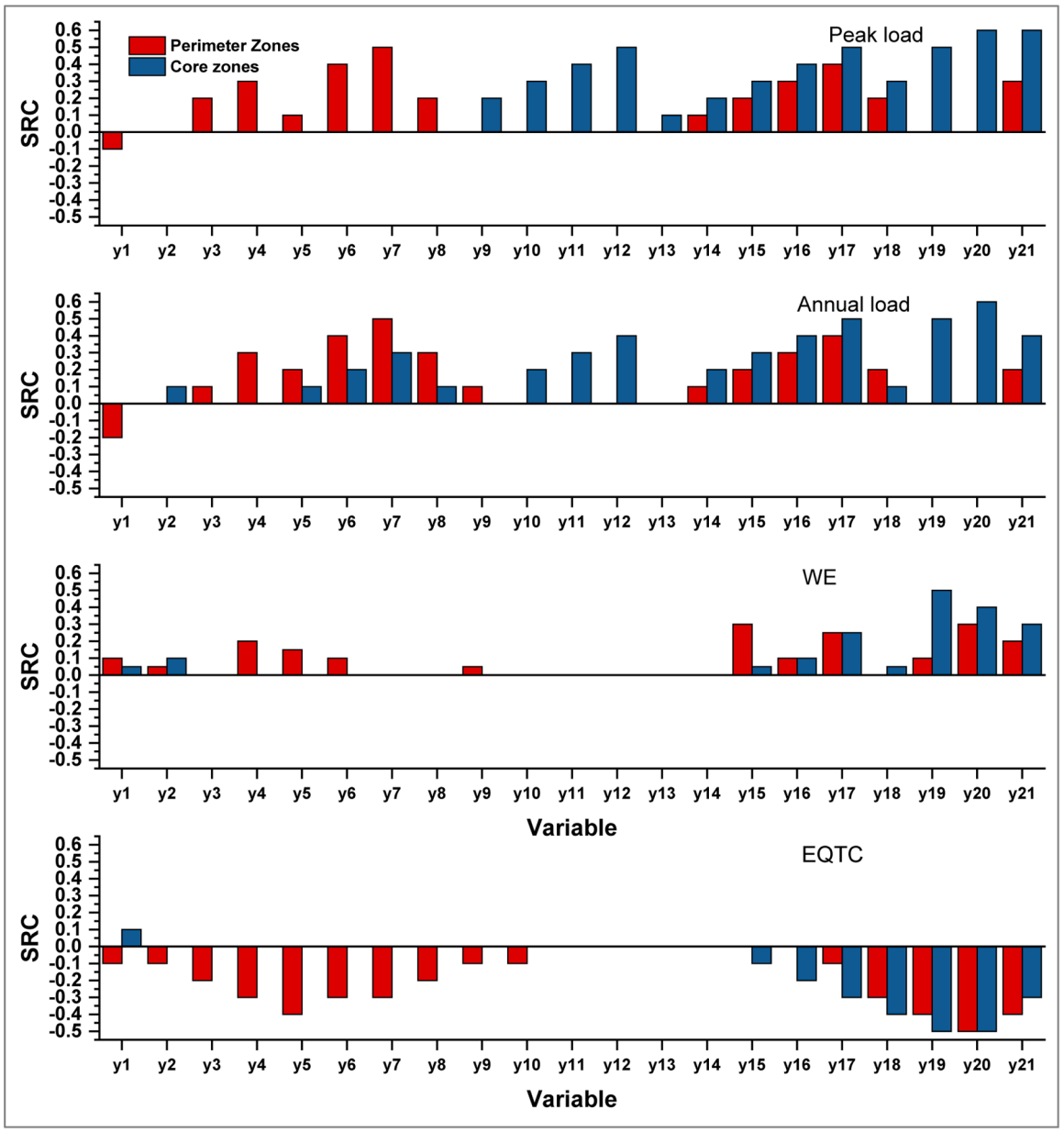


**Fig. 8.** The sensitivity analysis results indicating the varying impacts of different parameters on annual cooling load, peak load, WE, and EQTC in both perimeter and core zones.

and 0.5. The lowest sensitivity is that of y1, with a coefficient of −0.1, which indicates a very slight negative influence on peak load. The highest sensitivity in perimeter zones is that of y7, with a coefficient of 0.5, indicating a strong positive influence on peak load. In core zones, the coefficients range from 0 to 0.6. The most sensitive is y21 with a coefficient of 0.6, and the coefficients for a few parameters (y1, y2, y3) are equal to zero thus they do not affect the core zone.

### 3.4. Annual cooling load

Sensitivity analysis in the perimeter zones gives the coefficients between −0.2 and 0.5. The least sensitive is y1 with a coefficient of −0.2, and the most sensitive is y7 with a coefficient of 0.5. Core zones have coefficients between 0 and 0.6; the highest sensitivity in y20 at 0.6 suggests that this parameter imposes a strong positive influence. Similar to the peak load, some parameters (y1, y3) impose little or no effect on the annual cooling load within core zones.

From the sensitivity analysis, the coefficients for the perimeter zones are between 0 and 0.3. The most sensitive of all the perimeter zones is y15 at 0.3; hence, this has a very high positive effect on work efficiency. For the core zones, the sensitivities range between 0 and 0.5, with the highest being y19 at 0.5; hence, a strong positive impact on work efficiency. Coefficients representing many parameters in the core zones y3, y4 show zero coefficients, meaning they are not of importance in changing work efficiency.

For EQTC, the sensitivity coefficients range from −0.5 to 0 in the perimeter zones. For the perimeter zones, y20 has the most negative coefficient of −0.5, hence it exerts the strongest negative influence on EQTC. The core zones range from −0.5 to 0.1. In that regard, only y1 exhibits a feeble positive effect amounting to 0.1. Majority of the parameters have negative coefficients; thus, they pull down EQTC in the core zones.

Sensitivity analysis results show that the influences of different parameters on annual cooling load, peak load, work efficiency, and EQTC are different in both the perimeter and core zones. Parameters like y7, y20, and y21 have larger positive influences, especially in core zones,

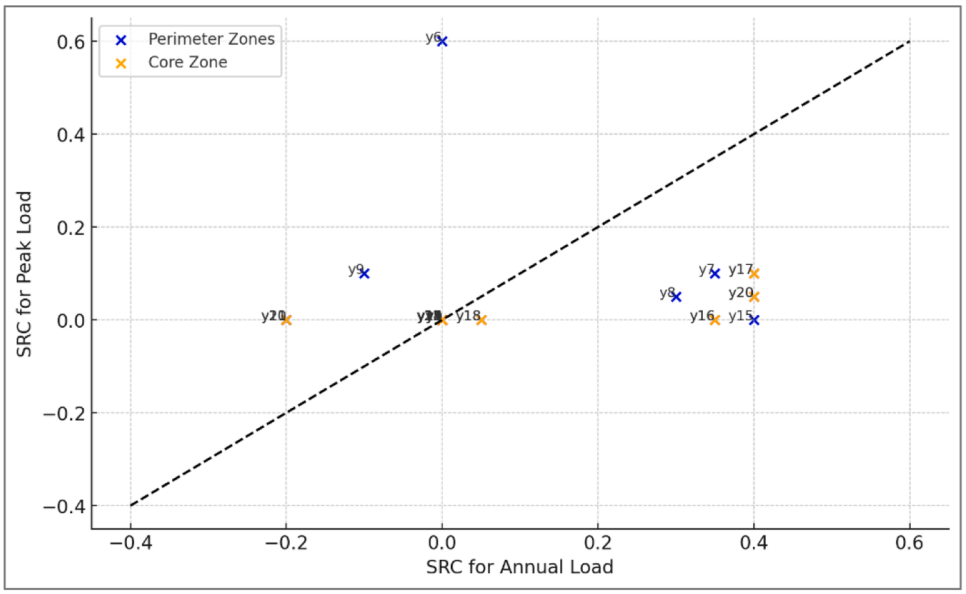


**Fig. 9.** The variables of SRC in peak load and annual load.

while parameters like y1 and y2 have lower or negative influences.

Sensitivity analysis results highlight the primary factors influencing annual cooling load and overall building performance. Among all variables, the Cooling Degree Days (CDD24) demonstrates the highest Standardized Regression Coefficient (SRC) for annual cooling load, confirming that climatic variations significantly affect cooling demands and reinforcing the necessity of accurate climate data integration in energy modeling. Global Solar Radiation (GSR) ranks second in sensitivity, underscoring the impact of solar gains on energy performance and the critical role of solar control strategies in reducing consumption.

Envelope-related variables including the overhang projection ratio, window-to-floor-area ratio, and orientation emerge as key determinants in regulating solar heat gain. The orientation parameter, with a peak cooling load SRC of 0.44, reveals a substantial influence on thermal load distribution. The Solar Heat Gain Coefficient (SHGC) also exhibits strong sensitivity, as it directly governs the transmission of solar radiation through fenestration, thereby affecting internal heat accumulation. Although the U-value of the envelope shows comparatively lower sensitivity, results suggest that insulation alone offers limited energy savings without concurrent passive design measures. Regarding internal conditions, the temperature set-point records the highest SRC for EQTC, indicating a significant impact on thermal comfort. Additional contributors include occupant density, lighting power density, and ventilation rate factors that collectively shape internal heat gains and thermal balance. In contrast, internal thermal mass demonstrates relatively low sensitivity, suggesting a minimal effect on comfort compared to other operational variables. These findings offer a data-driven basis for prioritizing design and operational strategies that optimize both energy efficiency and occupant well-being.

Fig. 9 shows the SRC for the annual load versus peak load relationship in different zones. The result reveals the features of load distribution and planning resource allocation efficiently across different zones. However, some variables such as room orientation (y6) exhibit divergent effects on annual versus peak cooling loads; that is, their

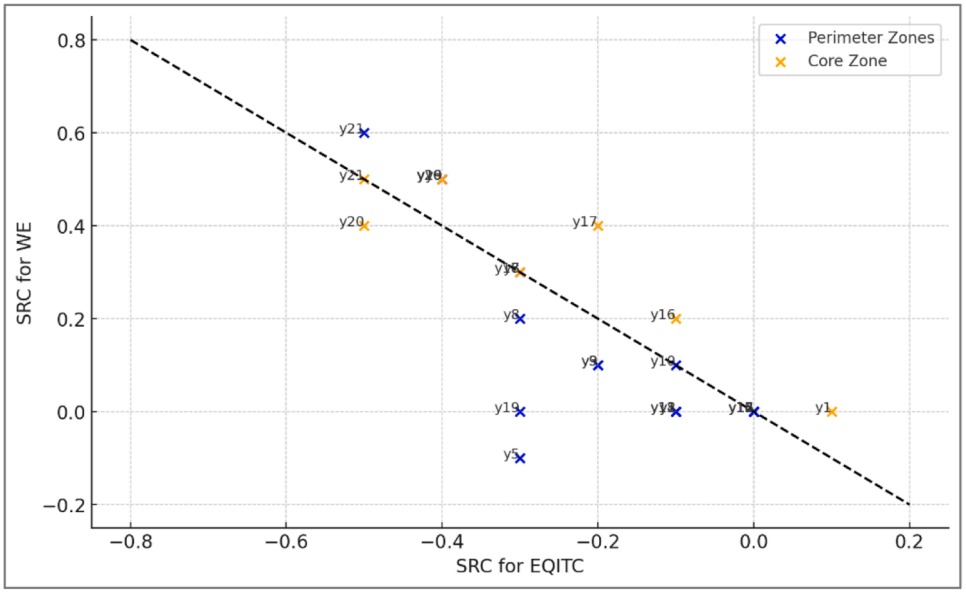


**Fig. 10.** The variables of SRC in WE and EQTC.

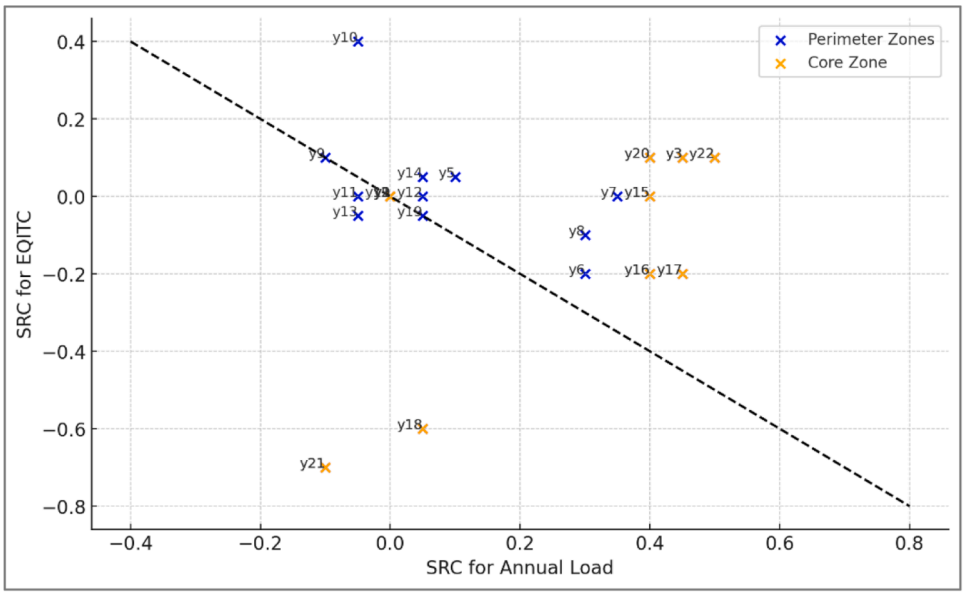


**Fig. 11.** The variables of SRC in EQTC and annual load.

relationship does not follow the diagonal line. This would suggest that room orientation is a more subtle factor, having different effects on building energy performance depending on whether the focus is on peak or annual loads.

Fig. 10 presents a scatterplot of SRC for WE and EQTC, revealing an inverse correlation between the two metrics. The SRC values exhibit similar magnitudes but opposite signs, indicating that variables contributing positively to one metric tend to negatively influence the other. The close alignment in absolute SRC values suggests that both output variables respond to the same set of inputs in a consistent yet opposing manner, highlighting a trade-off between optimizing energy efficiency and thermal comfort.

Fig. 11 Scatterplot of SRC for annual cooling and EiTC load versus different input variables. It was found that some of the variables have high values of SRC on both EQTC and annual cooling load, indicating their crucial importance in the overall building performance. Similarly, room orientation (y6), window area ratio (y7), SHGC (y8), and overhang projection ratio (y10) all have large SRC values, which impose great influence on both thermal comfort and energy consumption. The temperature set-point (y21) and ventilation rate (y20) also show large SRC values, especially in regard to EQTC, which indicates that precise control of these parameters is necessary to keep indoor comfort. The scatterplot emphasizes the fact that while some variables may have a strong effect on both EQTC and annual cooling load, the nature of the influence can be quite different. This double visualization helps to understand in detail how various design and operational factors contribute to both thermal comfort and energy efficiency and lead to optimal building performance strategies.

### 3.5. *Multi-Linear regression (MLR) model developed*

The MLR model was developed using the MLR method for the prediction of peak load and WE in buildings. The performance of the models was evaluated using various statistical metrics, including $R^2$ values, MAPE values, and CVRMSE values. The $R^2$ values represent the proportion of the variance in the dependent variable that is predictable from the independent variables, where higher values indicate better model fit. Stepwise regression technique with both forward and backward elimination of variables was also used for model development in this regard in order to present the most likely predictors of MRL. To begin with, the forward selection technique added all variables to a model one by one according to their contribution on the basis of performance and evaluated inclusion using Bayesian Information Criterion (BIC). The BIC prevents overfitting by penalizing the number of parameters in the model, ensuring that it only includes variables that provide a statistically significant improvement in the model. Overfitting occurs when the models are too complex and start capturing the noise in the data rather than the pattern of the data. Interpret results from the model: SRC were used to give a relative importance score to each predictor variable. The analysis showed that variables like GSR have an important impact on the peak load and WE model, hence proving the usefulness of the MLR approach in understanding and predicting building energy performance.

Table 5 displays the results of a stepwise regression analysis, including introduced variables with their respective regression coefficients, correlations, and statistical errors. Stepwise regression is one of the regression methods where the selection of the prediction variables is done through an automated procedure. The analysis highlights parameters that significantly influence peak load, annual load, WE, and EQTC within renewable energy models. These regression coefficients represent the strength and direction of the influence of each variable. This detailed breakdown in the critical factors affecting building energy performance informs the development of more efficient renewable energy models.

Results of a stepwise regression analysis are given in Table 5, where $R^2$ is an important metric presented for various dependent variables: peak load, annual load, WE, and EQTC. All $R^2$ values are very high, showing that models' predictions are precise and vary between 0.92 and 0.96 for peak load, 0.94 and 0.97 for annual load, 0.92 and 0.96 for WE, and 0.95 and 0.97 for EQTC. These $R^2$ values mean that the regression models explain a great deal of the variance in these variables, indicating their predictive power and reliability.

The MAPE and CVRMSE as measures of model accuracy and error. For the annual load, the MAPE falls within the range 1.6 % to 3.55 %, which is a low percentage error and an indication of high model precision. On the other hand, WE have a higher MAPE range of 12.3 % to 15.55 %, indicating greater variability and less precision in the predictions for WE. Similarly, the CVRMSE for annual load ranges between 1.1 % and 3.3 %, further emphasizing the accuracy of the model, while for WE, the CVRMSE ranges between 18.33 % and 25.5 %, further indicating higher error and lower reliability in the prediction of WE compared to the annual load. Percentages of explained variation for

**Table 5**
Analysis using stepwise regression, covering introduced variables, regression coefficients, correlations, and statistical errors.

| Parameter | Orientations | y0 | y2 | y3 | y5 | y7 | y8 | y9 | y10 | y11 | y15 | y16 | y17 | y18 | y20 | y21 | MAPE | CVRMSE | $R^2$ |
|---|---|---|---|---|---|---|---|---|---|---|---|---|---|---|---|---|---|---|---|
| Peak load | N | 85.53 | | | | 10.33 | 22.76 | | −2.44 | −0.002 | 0.96 | 0.91 | 98.05 | | 35.66 | −3.57 | 3.20 % | 4.50 % | 0.94 |
| | E | 77.94 | | | | 30.45 | 56.07 | | −30.67 | −0.002 | 0.95 | 0.93 | 92.21 | | 32.16 | −3.68 | 4.30 % | 6.40 % | 0.93 |
| | S | 86.42 | | | | 9.29 | 20.48 | | −1.53 | −0.002 | 0.94 | 0.93 | 97.78 | | 35.74 | −3.48 | 3.40 % | 4.60 % | 0.94 |
| | W | 72.54 | | | | 36.22 | 62.33 | | −25.59 | −0.001 | 1.06 | 0.92 | 101.45 | | 34.84 | −3.44 | 3.80 % | 5.90 % | 0.93 |
| | C | 57.65 | | | | | | | | | 1.07 | 0.94 | 97.97 | | 36.25 | −2.25 | 2.40 % | 4.50 % | 0.96 |
| Annual load | N | 112.14 | 3.22 | | | 10.98 | 50.32 | −3.34 | −6.88 | | 3.33 | 3.15 | 297.34 | | 52.88 | −13.44 | 1.70 % | 1.20 % | 0.98 |
| | E | 63.03 | 3.86 | | | 31.77 | 89.44 | −3.21 | −31.43 | | 3.55 | 3.08 | 307.66 | | 53.22 | −12.87 | 2.60 % | 1.60 % | 0.97 |
| | S | 36.65 | 4.23 | | | 33.68 | 87.67 | −3.87 | −41.89 | | 3.19 | 3.22 | 312.67 | | 55.47 | −12.37 | 3.50 % | 2.10 % | 0.94 |
| | W | 43.85 | 3.86 | | | 36.24 | 101.91 | −3.43 | −30.22 | | 3.68 | 3.34 | 309.52 | | 54.59 | −12.44 | 2.40 % | 3.50 % | 0.97 |
| | C | 62.52 | 2.45 | | | | | | | | 3.24 | 3.54 | 310.41 | | 50.88 | −8.59 | 1.80 % | 2.20 % | 0.98 |
| Annual load | N | −429.37 | 0.32 | −0.68 | −1.97 | 3.43 | 9.34 | | −1.53 | | 0.99 | 0.39 | 21.41 | 0.78 | | 12.87 | 12.80 % | 18.50 % | 0.97 |
| | E | −424.32 | 0.12 | 1.53 | −2.65 | 7.07 | 16.36 | | −6.53 | | 0.56 | 0.34 | 18.33 | 0.76 | | 12.63 | 13.70 % | 18.20 % | 0.96 |
| | S | −452.78 | 0 | 5.35 | −2.52 | 7.56 | 16.65 | | −8.22 | | 0.81 | 0.37 | 18.85 | 0.76 | | 13.24 | 15.80 % | 21.80 % | 0.94 |
| | W | −405.03 | 0.16 | 1.04 | −2.79 | 7.75 | 17.28 | | −5.95 | | 0.94 | 0.38 | 17.38 | 0.64 | | 12.21 | 14.40 % | 18.80 % | 0.95 |
| | C | −607.63 | | | | | | | | | 0.55 | 0.86 | 33.28 | 0.97 | | 18.98 | 15.60 % | 25.90 % | 0.96 |
| EQTC | N | 1062.21 | | −4.12 | | −6.37 | −20.55 | | 3.16 | | | −0.88 | | −1.85 | | −29.17 | 5.10 % | 6.80 % | 0.95 |
| | E | 1113.62 | | −8.23 | | −12.87 | | −33.39 | 11.57 | | | −0.84 | | −1.88 | | −30.25 | 6.70 % | 8.70 % | 0.96 |
| | S | 1161.05 | | −11.82 | | −13.74 | −32.88 | | 15.43 | | | −0.89 | | −1.97 | | −31.89 | 6.80 % | 8.50 % | 0.96 |
| | W | 1092.62 | | −8.67 | | −13.38 | −35.78 | | 10.99 | | | −0.84 | | −1.78 | | −29.92 | 6.40 % | 8.60 % | 0.96 |
| | C | 1343.13 | | | | | | | | | −1.10 | −1.63 | −73.77 | −2.23 | | −38.19 | 5.50 % | 7.60 % | 0.96 |

each variable further affirm the models' robustness. The peak load variation explained ranges from 91 % to 96 %, annual load from 92 % to 97 %, WE from 94 % to 96 %, and EQTC from 93 % to 96 %. The high percentages of explained variation underscore the effectiveness of the models in capturing the main trends and patterns in the data. Taken together, these metrics indicate that the models perform in a generally accurate and reliable way in predicting the respective variables, and that annual load and EQTC especially demonstrate strong performance metrics across all measures.

Table 6 presents a comparative analysis of validation metrics between the proposed predictive model and several established models from the literature. The summary underscores the model's robust performance in terms of accuracy and consistency, particularly when evaluated alongside other advanced simulation and machine learning frameworks.

Table 7 presents a comprehensive analysis conducted without applying stepwise regression, incorporating all input variables within the model framework. The reported correlation coefficients indicate the strength and direction of relationships among variables, while statistical performance indicators such as MAPE, CVRMSE, and $R^2$ are provided to assess model accuracy and reliability. This full-variable approach offers deeper insight into both direct and indirect effects, supporting evaluation of the model's robustness and predictive capability.

### *3.6. Comparison of linear regression models with/without interaction terms*

This section presents a comparative analysis of linear regression models with and without interaction terms, incorporating quadratic expressions to enhance predictive complexity and accuracy for building performance metrics. Model validity was evaluated using 650 independent simulation cases, assessing performance indicators such as peak load, annual load, WE, and EQTC. Accuracy verification against EnergyPlus simulation outputs confirmed the reliability and robustness of the proposed models.

- **Nonlinear terms and model accuracy**: Incorporating nonlinear terms into the regression model has significantly improved its accuracy. This enhancement is evident in the Mean Absolute Percentage Error (MAPE) reduction from 1.76 % to 1.42 %, indicating a more precise model. Additionally, the WE model, which assesses thermal comfort, shows a marked improvement in MAPE from 13.44 % to 9.52 %.
- **Simple linear models and peak load estimation**: While simple linear models are effective in estimating certain aspects such as peak load, as shown in subplot (a), where $R^2$ values are exceptionally high (0.97 and 0.99), they may not fully capture the intricacies of thermal comfort predictions. The $R^2$ values indicate a strong correlation between the predicted and actual peak load values, demonstrating the model's robustness in this area.
- **Simplified model for rapid assessment**: The simplified regression model with nonlinear terms offers a practical solution for rapid assessment of cooling demand during the design stages of building projects. This model allows for quick and accurate predictions without the need for extensive computational resources, making it an invaluable tool for architects and engineers. Leveraging this enhanced model, professionals can make informed decisions early in the design process, optimizing building performance and ensuring efficient energy usage.

Table 8, gives the performance metrics of the regression models. The results across the board are better for the model with interaction terms, mainly in terms of model accuracy and quality of fit. In terms of annual load and WE indicators, the model with interaction terms has lower MAPE and CVRMSE. This model also has higher R2 values for peak load and EQTC indicators, which shows that it is better able to capture

**Table 6**
Comparative validation metrics of the proposed predictive model with related literature.

| Study / Model | $R^2$ (Annual Load) | MAPE ( %) | CVRMSE ( %) | Validation Method / Tool | Reference |
|---|---|---|---|---|---|
| Current Study (MLR + Interaction Terms) | 0.98 | 1.59 | 1.47 | Monte Carlo + EnergyPlus | Present Study |
| Alghamdi et al. (2024) – ANN + Monte Carlo | >0.97 | <2.0 | – | ANN + EnergyPlus + Monte Carlo | [14] |
| Gabrielli and Ruggeri (2019) – Optimization model | 0.95 | 2.5 | 2.0 | Simulation + Uncertainty Analysis | [17] |
| Jafarpur & Berardi (2021) – Climate setpoint model | 0.94–0.97 | 1.6–9.1 | – | Energy simulation under climate scenarios | [19] |
| Rabani et al. (2021) – CFD + Daylight + Energy | – | ~2.0 | – | Coupled simulation models | [18] |

complicated cross-variable relationships and make more precise predictions.

### 3.7. Carbon emission reduction potential

Achieving Net-Zero Carbon status in the building sector necessitates not only minimizing energy consumption but also accurately quantifying the resulting carbon emission reductions. Simulation outcomes from the current study indicate significant decreases in annual cooling loads through optimization of key parameters such as indoor temperature set-point, glazing characteristics (SHGC and U-value), and window-to-floor area ratio. These energy savings translate directly into lower carbon emissions when applying the regional electricity carbon intensity. For instance, implementation of optimal temperature settings and passive architectural measures yielded cooling load reductions of up to 50 kWh/$m^2$ annually. With an emission factor of 0.45 kg $CO_2$/kWh, this corresponds to an estimated carbon reduction of 22.5 kg $CO_2/m^2$/year. Table 9 provides a summary of estimated emission reductions under various retrofit scenarios.

## 4. Conclusions

This study introduced a comprehensive predictive modeling framework designed to evaluate and optimize building energy consumption and indoor thermal comfort, with a specific emphasis on achieving Net-Zero Carbon targets. A detailed case study was conducted on a typical office building exposed to three distinct climatic conditions Baghdad, Basra, and Mosul using actual weather data and a range of 21 design and operational parameters. The objective was to assess and enhance cooling load performance and thermal comfort through targeted design and retrofitting strategies. The methodology integrated EnergyPlus simulations with Monte Carlo analysis and multi-linear regression (MLR) models incorporating both interaction and quadratic terms [63,64]. This enabled the capture of nonlinear relationships between critical design variables including SHGC, indoor temperature set-point, and window-to-floor area ratio and key performance indicators such as annual and peak cooling load, WE, and the EQTC index. The Results key findings:

- The developed predictive model demonstrated high accuracy, with $R^2$ is 0.98, MAPE is 1.59 %, and CVRMSE is 1.47 %, confirming its reliability in estimating cooling loads and thermal comfort metrics.
- Optimizing the indoor temperature set-point from 24 °C to 26 °C reduced the peak cooling load from 125 W/$m^2$ to 95 W/$m^2$, contributing to significant energy savings without compromising comfort.
- Reducing the SHGC from 0.9 to 0.4 resulted in a decrease in annual cooling demand of up to 50 kWh/$m^2$, highlighting the effectiveness of glazing performance improvements.
- Combined retrofitting strategies optimizing set-point temperature, SHGC, and glazing U-value achieved total annual energy savings of up to 70 kWh/$m^2$.
- These energy savings correspond to a potential carbon emission reduction of 31.5 kg $CO_2/m^2$/year, based on a regional emission factor of 0.45 kg $CO_2$/kWh.
- The EQTC index improved from 50 to 100 under optimal design configurations, indicating a substantial enhancement in indoor comfort.
- Spatial performance analysis showed higher cooling loads in perimeter zones (up to 198 W/$m^2$) compared to core zones (as low as 106 W/$m^2$), emphasizing the importance of zone-specific HVAC and design strategies.

The outcomes validate the effectiveness of the modeling framework as a decision-support tool for enhancing energy efficiency, thermal comfort, and carbon reduction in building design and retrofitting. The approach is scalable, adaptable to diverse climate zones, and applicable for use by architects, engineers, and policymakers advancing Net-Zero Carbon building initiatives.

## Study limitations

Despite comprehensive modeling techniques and extensive validation processes, several limitations remain. The predictive framework primarily relies on simulation data and does not incorporate real-time adaptive behavior or occupancy variability beyond predefined scenarios. Climatic inputs were restricted to selected cities within a specific geographical region, potentially limiting the generalizability of the findings to broader climate zones. The Monte Carlo analysis, while robust, utilized fixed parameter distributions that may not fully reflect the dynamic fluctuations found in real-world building environments. Furthermore, the model focused predominantly on cooling loads and did not extensively account for heating requirements or seasonal thermal performance variability. The EQTC metric, although comprehensive, is subject to assumptions inherent in the PMV-PPDI model, which may not fully capture the subjective comfort perceptions of all occupants. Future extensions may address these gaps through integration of real-time building performance data, broader climatic datasets, and advanced comfort modeling techniques incorporating behavioral and adaptive responses.

## CRediT authorship contribution statement

**Sameer Algburi:** Investigation, Methodology, Writing – original draft. **Aymen Mohammed:** Resources, Validation, Supervision. **Ibrahim Abdullah:** Data curation, Visualization, Software. **Talib Munshid Hanoon:** Project administration, Supervision, Writing – review & editing. **Hassan Falah Fakhruldeen:** Methodology, Formal analysis. **Otabek Mukhitdinov:** Software, Validation. **Feryal Ibrahim Jabbar:** Writing – review & editing, Resources. **Qusay Hassan:** Conceptualization, Supervision, Funding acquisition. **Ali Khudhair:** Investigation, Data curation. **David Kato:** Formal analysis, Data curation, Conceptualization.

## Declaration of competing interest

The authors declare that they have no known competing financial interests or personal relationships that could have appeared to influence the work reported in this paper.

**Table 7**
Comprehensive analysis excluding stepwise regression, featuring included variables, regression coefficients, correlations, and statistical errors.

| Parameter | Orientations | y0 | y2 | y3 | y5 | y9 | y11 | y15 | y16 | y17 | y18 | y20 | y21 | y7y10 | y7y8 | y8y10 | y17y18 | y18y21 | $y18^2$ | $x21^2$ | MAPE | CVRMSE | $R^2$ |
|---|---|---|---|---|---|---|---|---|---|---|---|---|---|---|---|---|---|---|---|---|---|---|---|
| Peak load | N | 99.25 | | | | | 1.22 | 1.12 | 1.02 | 0.92 | 99.88 | | 36.31 | −3.57 | | 17.34 | −5.2 | | | | 3.02 % | 3.71 % | 0.95 |
| | E | 109.75 | | | | | 1.34 | 1.63 | 1.02 | 0.82 | 94.69 | | 32.95 | −3.77 | | 53.86 | −52.43 | | | | 3.53 % | 4.40 % | 0.96 |
| | S | 99.05 | | | | | 1.57 | 1.02 | 1.02 | 0.92 | 99.45 | | 36.51 | −3.57 | | 15.1 | −2.45 | | | | 2.97 % | 3.66 % | 0.95 |
| | W | 111.18 | | | | | 2.22 | 2.14 | 1.02 | 0.92 | 102.81 | | 35.7 | −3.77 | | 58.54 | −44.27 | | | | 3.47 % | 4.29 % | 0.96 |
| | C | 57.73 | | | | | | 1.02 | 0.92 | | 99.35 | | 37.02 | −2.14 | | | | | | | 2.99 % | 3.70 % | 0.97 |
| Annual load | N | 134.96 | 3.41 | | −3.53 | −3.42 | | 3.45 | 3.22 | | 54.01 | −13.51 | 52.01 | −13.52 | 29.27 | −7.82 | 2.6 | | | | 2.06 % | 2.56 % | 0.99 |
| | E | 107.5 | 3.86 | | −3.32 | −3.11 | | 3.48 | 3.18 | | 55.17 | −13.37 | 67.64 | −49.17 | 2.71 | | | | | | 2.59 % | 3.23 % | 0.98 |
| | S | 78.6 | 4.25 | | −3.15 | −3.22 | | 3.53 | 3.13 | | 56.7 | −13.23 | 71.09 | −66.4 | 2.76 | | | | | | 3.54 % | 4.34 % | 0.96 |
| | W | 94.91 | 4.04 | | −3.49 | −3.55 | | 3.49 | 3.18 | | 55.63 | −13.3 | 75.09 | −48.27 | 2.72 | | | | | | 2.50 % | 3.12 % | 0.97 |
| | C | 65.69 | 2.37 | | | | | 3.75 | 3.65 | | 51.63 | −8.52 | | 2.66 | | | | | | | 1.59 % | 2.06 % | 0.96 |
| WE | N | 2619.39 | 0.18 | −0.48 | −1.76 | | | 0.22 | 0.37 | 20.43 | −8.71 | | −183.02 | 5.71 | −1.93 | 0.32 | 0.005 | 3.1 | 10.84 % | 18.01 % | 0.99 | 4.29 % | 0.95 |
| | E | 2583.82 | 0.15 | 1.08 | −2.33 | | | 0.2 | 0.3 | 16.96 | −8.63 | | −182.53 | 12.44 | −8.21 | 0.34 | 0.003 | 3.09 | 11.70 % | 16.11 % | 0.98 | 3.70 % | 0.96 |
| | S | 2932.26 | 0.02 | 4.03 | −2.17 | | | 0.22 | 0.33 | 17.3 | −10.05 | | −204 | 12.21 | −11.64 | 0.39 | 0.004 | 3.42 | 12.66 % | 17.97 % | 0.97 | 2.56 % | 0.97 |
| | W | 2965.65 | 0.02 | 4.21 | −2.16 | | | 0.22 | 0.34 | 18.13 | −10.28 | | −205.61 | 12.29 | −11.88 | 0.39 | 0.005 | 3.43 | 13.77 % | 20.10 % | 0.98 | 3.23 % | 0.96 |
| | C | −7443.56 | | | | | | 0.56 | 0.94 | 39.77 | 26.34 | | 434.31 | | | | −0.74 | −0.03 | −6.38 | 9.69 % | 18.14 % | 0.98 | 0.97 |
| EQTC | N | 588.59 | | −4.29 | | | | | −0.88 | | | | 2.26 | −13.2 | −0.26 | 0.02 | | | | | 4.80 % | 6.49 % | 0.97 |
| | E | 616.67 | | −8.58 | | | | | −0.87 | | | | 7.09 | −24.4 | −0.27 | 0.02 | | | | | 6.58 % | 8.42 % | 0.97 |
| | S | 648.86 | | −12.28 | | | | | −0.9 | | | | 9.17 | −25.23 | −0.28 | 0.02 | | | | | 6.55 % | 8.45 % | 0.97 |
| | W | 605.07 | | −9 | | | | | −0.86 | | | | 6.44 | −25.33 | −0.26 | 0.02 | | | | | 6.81 % | 8.60 % | 0.98 |
| | C | 706.51 | | | | | | | −1.07 | −1.61 | −68.96 | | | −0.33 | 0.03 | | | | | 5.87 % | 7.90 % | 0.97 | 0.97 |

**Table 8**
Performance metrics comparison with/without more interaction terms.

| Indicator | Metric | CVRMSE | MAPE | $R^2$ |
|---|---|---|---|---|
| With interaction terms | Peak load | 2.46 % | 2.75 % | 0.99 |
| | Annual load | 1.47 % | 1.59 % | 0.98 |
| | WE | 10.11 % | 9.31 % | 0.97 |
| | EQTC | 5.15 % | 5.37 % | 0.99 |
| Without interaction terms | Peak load | 2.45 % | 2.75 % | 0.98 |
| | Annual load | 1.58 % | 1.69 % | 0.99 |
| | WE | 13.44 % | 12.64 % | 0.98 |
| | EQTC | 5.31 % | 5.56 % | 0.98 |

**Table 9**
Estimated carbon emission reduction under selected retrofitting scenarios.

| Scenario description | Cooling load reduction (kWh/$m^2$/year) | Emission factor (kg $CO_2$/kWh) | Carbon reduction (kg $CO_2/m^2$/year) |
|---|---|---|---|
| Optimized Indoor Temp. Set-Point (26 °C) | 40 | 0.45 | 18 |
| SHGC Reduced from 0.9 to 0.4 | 50 | 0.45 | 22.5 |
| Improved Glazing U-value (5.8 - 1.8 W/$m^2$·K) | 35 | 0.45 | 15.75 |
| Window-to-Floor Area Ratio Optimization | 30 | 0.45 | 13.5 |
| Combined Measures (Integrated Design Package) | 70 | 0.45 | 31.5 |

## Data availability

No data was used for the research described in the article.

## References

[1] D. Ürge-Vorsatz, R. Khosla, R. Bernhardt, Y.C. Chan, D. Vérez, S. Hu, L.F. Cabeza, Advances toward a net-zero global building sector, Annu. Rev. Env. Resour. 45 (2020) 227–269.

[2] S. Barbhuiya, B.B. Das, D. Adak, Roadmap to a net-zero carbon cement sector: strategies, innovations and policy imperatives, J. Env. Manage 359 (2024) 121052.

[3] J. Friedmann, A. Zapantis, B. Page, C. Consoli, Z. Fan, I. Havercroft, A. Townsend, Net-zero and Geospheric return: Actions Today for 2030 and Beyond, Columbia University, Center on Global Energy Policy, 2020.

[4] F. Johnsson, I. Karlsson, J. Rootzén, A. Ahlbäck, M. Gustavsson, The framing of a sustainable development goals assessment in decarbonizing the construction industry–avoiding "greenwashing, Renew. Sustain. Energy Rev. 131 (2020) 110029.

[5] A. Garvey, J.B. Norman, J. Barrett, Technology and material efficiency scenarios for net zero emissions in the UK steel sector, J. Clean. Prod. 333 (2022) 130216.

[6] S. Mirzabeigi, R. Zhang, B. Krietemeyer, of an integrated whole-building energy efficiency Retrofit assembly, in: Multiphysics and Multiscale Building Physics: Proceedings of the 9th International Building Physics Conference (IBPC 2024) Volume 2: Urban Physics and Energy Efficiency, Springer Nature, 2025, p. p. 73.

[7] V.J. Reddy, N.P. Hariram, M.F. Ghazali, S. Kumarasamy, Pathway to sustainability: an overview of renewable energy integration in building systems, Sustainability 16 (2) (2024) 638.

[8] Sachs, L., Mardirossian, N., & Toledano, P. (2023). Finance for zero: redefining financial-sector action to achieve global climate goals. *Available at SSRN* 4512376.

[9] K. Chatzikonstantinidis, N. Afxentiou, E. Giama, P.A. Fokaides, A. M. Papadopoulos, Energy management of smart buildings during crises and digital twins as an optimisation tool for sustainable urban environment, Int. J. Sustain. Energy 44 (1) (2025) 2455134.

[10] C. Deb, A. Schlueter, Review of data-driven energy modelling techniques for building retrofit, Renew. Sustain. Energy Rev. 144 (2021) 110990.

[11] A. Albatayneh, D. Alterman, A. Page, B. Moghtaderi, The impact of the thermal comfort models on the prediction of building energy consumption, Sustainability 10 (10) (2018) 3609.

[12] M.M. Saad, R.P. Menon, U. Eicker, Supporting decision making for building decarbonization: developing surrogate models for multi-criteria building retrofitting analysis, Energies 16 (16) (2023) 6030.

[13] V.A. Arowoiya, R.C. Moehler, Y. Fang, Digital twin technology for thermal comfort and energy efficiency in buildings: a state-of-the-art and future directions, Energy Built Environ. (2023).

[14] S. Alghamdi, W. Tang, S. Kanjanabootra, D. Alterman, Optimising building energy and comfort predictions with intelligent computational model, Sustainability 16 (8) (2024) 3432.
[15] M. Braulio-Gonzalo, M.D. Bovea, M.J. Ruá, P. Juan, A methodology for predicting the energy performance and indoor thermal comfort of residential stocks on the neighbourhood and city scales. A case study in Spain, J. Clean. Prod. 139 (2016) 646–665.
[16] M. Santamouris, K. Vasilakopoulou, Present and future energy consumption of buildings: challenges and opportunities towards decarbonisation. *E-prime-advances in Electrical engineering*, Electron. Energy 1 (2021) 100002.
[17] L. Gabrielli, A.G. Ruggeri, Developing a model for energy retrofit in large building portfolios: energy assessment, optimization and uncertainty, Energy Build. 202 (2019) 109356.
[18] M. Rabani, H. Bayera Madessa, N. Nord, Building retrofitting through coupling of building energy simulation-optimization tool with CFD and daylight programs, Energies 14 (8) (2021) 2180.
[19] P. Jafarpur, U. Berardi, Effects of climate changes on building energy demand and thermal comfort in Canadian office buildings adopting different temperature setpoints, J. Build. Eng. 42 (2021) 102725.
[20] F. Martín-Consuegra, C.A. Ludueña, F. De Frutos, B. Frutos, C. Alonso, I. Oteiza, Expectations and outcomes when quantifying energy improvements achieved by building envelope retrofitting, Sustainability 16 (8) (2024) 3214.
[21] G.R. Araújo, R. Gomes, P. Ferrão, M.G. Gomes, Optimizing building retrofit through data analytics: a study of multi-objective optimization and surrogate models derived from energy performance certificates, Energy Built Environ. (2023).
[22] K.W. Mui, L.T. Wong, M.K. Satheesan, I. Ibragimov, A hybrid simulation model to predict the cooling energy consumption for residential housing in Tashkent, Energies 14 (16) (2021) 4850.
[23] L. Walker, I. Hischier, A. Schlueter, Does context matter? Robust building retrofit decision-making for decarbonization across Europe, Build Env. 226 (2022) 109666.
[24] G. Aruta, F. Ascione, N. Bianco, G.M. Mauro, G.P. Vanoli, Optimizing heating operation via GA-and ANN-based model predictive control: concept for a real nearly-zero energy building, Energy Build. 292 (2023) 113139.
[25] J. Shi, W. Chen, X. Yin, Modelling building's decarbonization with application of China TIMES model, Appl. Energy 162 (2016) 1303–1312.
[26] M. Jradi, B.E. Madsen, J.H. Kaiser, DanRETwin: a digital twin solution for optimal energy retrofit decision-making and decarbonization of the Danish building stock, Appl. Sci. 13 (17) (2023) 9778.
[27] É. Mata, J. Wanemark, V.M. Nik, A.S. Kalagasidis, Economic feasibility of building retrofitting mitigation potentials: climate change uncertainties for Swedish cities, Appl. Energy 242 (2019) 1022–1035.
[28] C.M.M. González, A.L. Rodríguez, R.S. Medina, J.R. Jaramillo, Effects of future climate change on the preservation of artworks, thermal comfort and energy consumption in historic buildings, Appl. Energy 276 (2020) 115483.
[29] I.G. Dino, C.M. Akgül, Impact of climate change on the existing residential building stock in Turkey: an analysis on energy use, greenhouse gas emissions and occupant comfort, Renew. Energy 141 (2019) 828–846.
[30] K. Qu, X. Chen, Y. Wang, J. Calautit, S. Riffat, X. Cui, Comprehensive energy, economic and thermal comfort assessments for the passive energy retrofit of historical buildings-A case study of a late nineteenth-century victorian house renovation in the UK, Energy 220 (2021) 119646.
[31] F.R. Cecconi, A. Khodabakhshian, L. Rampini, Data-driven decision support system for building stocks energy retrofit policy, J. Build. Eng. 54 (2022) 104633.
[32] Z. Lin, T. Hong, X. Xu, J. Chen, W. Wang, Evaluating energy retrofits of historic buildings in a university campus using an urban building energy model that considers uncertainties, Sustain. Cities. Soc. 95 (2023) 104602.
[33] T. Tamer, I.G. Dino, C.M. Akgül, Data-driven, long-term prediction of building performance under climate change: building energy demand and BIPV energy generation analysis across Turkey, Renew. Sustain. Energy Rev. 162 (2022) 112396.
[34] Y. Xu, C. Yan, G. Wang, J. Shi, K. Sheng, J. Li, Y. Jiang, Optimization research on energy-saving and life-cycle decarbonization retrofitting of existing school buildings: a case study of a school in Nanjing, Sol. Energy 254 (2023) 54–66.
[35] E. Thrampoulidis, K. Orehounig, G. Hug, Electricity demand flexibility potential of optimal building retrofit solutions, in: Journal of Physics: Conference Series 2042, IOP Publishing, 2021 012149.
[36] H. Jia, A. Chong, eplusr: a framework for integrating building energy simulation and data-driven analytics, Energy Build. 237 (2021) 110757.
[37] N.R.M. Sakiyama, L. Mazzaferro, J.C. Carlo, T. Bejat, H. Garrecht, Dataset of the EnergyPlus model used in the assessment of natural ventilation potential through building simulation, Data Br. (2021) 34.
[38] M. Jradi, A decision-making tool for sustainable energy planning and retrofitting in Danish communities and districts, Energies (Basel) 18 (3) (2025) 692.
[39] D.S.K. Karunasingha, Root mean square error or mean absolute error? Use their ratio as well, Inf. Sci. (Ny) 585 (2022) 609–629.
[40] Q. Zhao, T. Hastie, Causal interpretations of black-box models, J. Bus. Econ. Stat. 39 (1) (2021) 272–281.
[41] C. Liu, H. Mohammadpourkarbasi, S. Sharples, Life cycle carbon and cost assessments of the retrofit to Passivhaus EnerPHit standard of suburban residential buildings in Hunan, China, Energy Build. (2025) 115417.
[42] N. Ma, D. Aviv, H. Guo, W.W. Braham, Measuring the right factors: a review of variables and models for thermal comfort and indoor air quality, Renew. Sustain. Energy Rev. 135 (2021) 110436.
[43] L.R. Jia, J. Han, X. Chen, Q.Y. Li, C.C. Lee, Y.H. Fung, Interaction between thermal comfort, indoor air quality and ventilation energy consumption of educational buildings: a comprehensive review, Buildings 11 (12) (2021) 591.
[44] S. Al-Saegh, V. Kourgiozou, I. Korolija, R. Tang, F. Tahmasebi, D. Mumovic, Investigating building stock energy and occupancy modelling approaches for district-level heating and cooling energy demands estimation in a university campus, Energy Build. (2025) 115269.
[45] W. Li, C. Koo, T. Hong, J. Oh, S.H. Cha, S. Wang, A novel operation approach for the energy efficiency improvement of the HVAC system in office spaces through real-time big data analytics, Renew. Sustain. Energy Rev. 127 (2020) 109885.
[46] C. Camarasa, É. Mata, J.P.J. Navarro, J. Reyna, P. Bezerra, G.B. Angelkorte, K. Yaramenka, A global comparison of building decarbonization scenarios by 2050 towards 1.5–2°C targets, Nat. Commun. 13 (1) (2022) 3077.
[47] Q. Hassan, S. Algburi, A.Z. Sameen, J. Tariq, A.K. Al-Jiboory, H.M. Salman, M. Jaszczur, A comprehensive review of international renewable energy growth, Energy Built Environ. (2024).
[48] R. Felez, J. Felez, Advanced energy management for residential buildings optimizing costs and efficiency through thermal energy storage and predictive control, Appl. Sci. 15 (2) (2025) 880.
[49] C. Suresh, T.K. Hotta, S.K. Saha, Phase change material incorporation techniques in building envelopes for enhancing the building thermal comfort-A review, Energy Build. 268 (2022) 112225.
[50] Q. Hassan, S. Algburi, A.Z. Sameen, H.M. Salman, M. Jaszczur, A review of hybrid renewable energy systems: solar and wind-powered solutions: challenges, opportunities, and policy implications, Results. Eng. (2023) 101621.
[51] Z. Zuo, J. Wang, M.A. Alghassab, N.A. Othman, A. Almadhor, F.M. Alhomayani, A. Eladeb, Heat *Re*-process approach and thermally integrated renewable energy system for power, compressed hydrogen, and freshwater production; ANN boosted optimization and techno-enviro-economic analysis, Case Stud. Therm. Eng. 66 (2025) 105748.
[52] C. Rodrigues, S. Usanov, M.S. Fernandes, S. Tadeu, Prospective life cycle approach to buildings' adaptation for future climate and decarbonization scenarios, Appl. Energy 372 (2024) 123867.
[53] M. Jia, R. Srinivasan, Building performance evaluation using coupled simulation of EnergyPlus™ and an occupant behavior model, Sustainability 12 (10) (2020) 4086.
[54] M.M. Saad, O. Otamurodov, U. Eicker, Supporting decision making for building decarbonization: developing surrogate models for multi-criteria building retrofitting analysis, Energies 16 (16) (2023) 6030.
[55] T. Ibrahim, Y. Omar, F.A. Maghraby, Water demand forecasting using machine learning and time series algorithms, in: 2020 International Conference on Emerging Smart Computing and Informatics (ESCI), IEEE, 2020, pp. 325–329.
[56] Q. Hassan, S. Algburi, A.Z. Sameen, M. Jaszczur, H.M. Salman, Hydrogen as an energy carrier: properties, storage methods, challenges, and future implications, Environ. Syst. Decis. (2023) 1–24.
[57] G. Yasmin, U. Gupta, An improved supervised machine learning model for gold price prediction, in: AIP Conference Proceedings 2919, AIP Publishing, 2024.
[58] M. Ghasaban, P. Mirjalili, M. Yeganeh, Integration of building envelope with open spaces and greenery to enhance thermal and visual comfort and energy efficiency in office buildings, Results. Eng. 25 (2025) 103660.
[59] L.F. Cabeza, M. Chàfer, Technological options and strategies towards zero energy buildings contributing to climate change mitigation: a systematic review, Energy Build. 219 (2020) 110009.
[60] X. Zhen, S. Li, J. Peng, Z. Zhao, X. Zhang, C. Tan, W. Wu, Analysis of building envelope for energy consumption and indoor comfort in a near-zero-energy building in Northwest China, Results. Eng. (2025) 104243.
[61] M.S. Geraldi, E. Ghisi, Building-level and stock-level in contrast: a literature review of the energy performance of buildings during the operational stage, Energy Build. 211 (2020) 109810.
[62] J. Moosanezhad, A. Basem, A.G. Alkhayer, A.H. Al-Rubaye, M. Khosravi, H. Azarinfar, Day-ahead resilience-economic energy management and feeder reconfiguration of a CCHP-based microgrid, considering flexibility of supply, Heliyon. (11) (2024) 10.
[63] A.M. Daabo, S. Zubeer, H. Ismaeel, F. Mustafa, H. Hamzah, A. Basem, H. Easa, A novel economic and technical dispatch model for household photovoltaic system considering energy storage system in "Duhok" City/Iraq as a case study, J. Energy Storage 94 (2024) 112440.
[64] A. Abdulsitar, N. Hasan, A. Basem, A. Daabo, A. Yaseen, H. Hamzah, Experimental study of the thermal performance of spiral flow solar water heating system, MRS Energy Sustain. 11 (2) (2024) 554–564.